CFD Letters

Journal homepage:
https://semarakilmu.com.my/journals/index.php/CFD_Letters/index
ISSN: 2180-1363

Entropy Generation and Heat Transfer Rate for MHD Forced Convection of Nanoliquid in Presence of Viscous Dissipation Term

Rached Miri[1], Bouchmel Mliki[1], Barhm Abdullah Mohamad[2], Mohamed Ammar Abbassi[1,*], Mowffaq Oreijah[3], Kamel Guedri[3], Souad Abderafi[4]

[1] Research Lab, Technology Energy and Innovative Materials, Faculty of Sciences, University of Gafsa, Tunisia
[2] Department of Petroleum Technology, Koya Technical Institute, Erbil Polytechnic University, 44001 Erbil, Iraq
[3] Mechanical Engineering Department, College of Engineering and Islamic Architecture, Umm Al-Qura University, P. O. Box 5555, Makkah 21955, Saudi Arabia
[4] Modeling of Energy Systems, Mechanical Materials and Structures, and Industrial Processes (MOSEM2PI), Mohammadia Engineering School, Mohammed V University in Rabat, Rabat, Morocco

ARTICLE INFO

Article history:
Received 14 May 2023
Received in revised form 12 June 2023
Accepted 13 July 2023
Available online 1 December 2023

Keywords:
Forced convection; Nanoliquid; Lattice Boltzmann method; Entropy generation Magnetohydrodynamic; Viscous dissipation

ABSTRACT

In this paper, magnetohydrodynamic laminar forced convection of nanoliquid in a rectangular channel with an extended surface, top moving wall and three cylindrical blocks is numerically studied. The Lattice Boltzmann method is used for the resolution of the governing equations. Validity of the numerical home elaborated FORTRAN code was made and good agreement was found with published results. It is interspersed in this work by the effects of the following parameters: Reynolds number ($50 \le Re \le 200$), Hartmann number ($0 \le Ha \le 50$), nanoparticles volume fraction ($0 \le \phi \le 4\%$) and Eckert number ($0.25 \le Ec \le 1$). The numerical solution shows that the local and average Nusselt numbers ameliorate when the value of Reynolds number, Eckert number, and the nanoparticles volume fraction are enhanced. But decreases when the Hartmann number is increased. The impacts of viscous dissipation on heat transfer rate and entropy generation are more noticeable in the presence of a magnetic field. The addition of 4% of nanoparticles enhances the local Nusselt number by about 7%.

1. Introduction

The optimization of heat transfer is an objective to be achieved. Many researchers have been interested in this subject because of its importance in the industry. The addition of nanoparticles in conventional fluids is one solution among several to improve the heat transfer rate. This solution is called nanofluid, which was proposed for the first time by Choi *et al.,* [1] The experimental results show that the addition of nanoparticles enhances the thermal conductivity of fluids. The impacts of solid volume fraction and temperature on thermal conductivity of DWCNT- ZnO/water-ethylene

* *Corresponding author.*
E-mail address: abbassima@gmail.com (Mohamed Ammar Abbassi)

https://doi.org/10.37934/cfdl.15.12.77106

glycol has been experimentally investigated by Mohammad *et al.,* [2]. The results disclosed that the thermal conductivity of nanofluid enhances with increasing concentration of nanoparticles. The influence of addition of Cu nanoparticles in base fluid on the thermal entropy generation and the frictional entropy generation has been studied by Farzad *et al.,* [3]. They concluded that the increasing of the nanoparticle volume fraction decreases the thermal entropy generation and increases the frictional entropy generation. The effects of addition of CNTs/Al2O3 nanoparticles in base fluid on thermal conductivity has been studied by Mohammad *et al.,* [4]. The numerical solution shows that the thermal conductivity of nanofluid depends directly on the solid volume fraction. Also, many numerical and experimental studies have been carried out on the effectiveness of nanofluids taken from previous studies [2-14]. They concluded that the addition of any type of nanoparticles (with thermal conductivity higher than that of base fluid) to base liquids enhances the thermal conductivity. Other works which are interesting in the use of nanofluids in heat exchangers can be found in Ref. [15-20]. The results demonstrated that the use of nanofluids has a positive impact on heat transfer in heat exchangers.

Applying a magnetic field to nanofluid forced convection has many effects on heat transfer. Magnetohydrodynamic (MHD) forced convection of nanofluid is one of the interesting topics for many researchers. This is due to important engineering applications such as nuclear reactors, heat exchangers, hydrodynamical machines, car radiators, and medical applications. In this context, the study of Karimipour *et al.,* [21] investigated numerically the laminar MHD forced convection flow of nanofluid (water/FMWNT carbon nanotubes) in a microchannel imposed to uniform heat flux. The results have shown that the fully developed velocity profile varied with Hartmann numbers. This means that increasing the magnetic field strength in order to increase the heat transfer rate is applicable only in a limited range, and it is not effective beyond that range. Forced convective heat transfer of nanofluids in porous half-rings has been studied in the presence of a uniform magnetic field by Sheikholeslami *et al.,* [22]. The results indicated that the Nusselt numbers decreased with the increase in Lorentz forces. The research work of Aminossadati *et al.,* [23] studied the magnetic field impact on forced convection of Al2O3 -water in a partially heated microchannel. The results reported that the microchannels are better in terms of heat transfer for higher Reynolds and Hartmann numbers. The effect of a magnetic field on free convection of three types of nanofluids: (copper/water, alumina/water and silver/water) has been studied by Hamad *et al.,* [24]. The numerical results show that the increase in the values of the magnetic parameters leads to a diminution of the velocity magnitude and to the parameter heat transfer rate for fixed values of nanoparticles concentrations. The influence of the external magnetic field on forced convection of ferrofluid (Fe3O4–water) is taken from the study by Sheikholeslami *et al.,* [25]. They found that the Nusselt number is a decreasing function of the Hartmann number. Selimefendigil *et al.,* [26] interspersed by the role of magnetic field in forced convection of CuO-water. The results demonstrate that the Hartmann number has positive effects on the average Nusselt number, and it was varied with the inclination angle of the lower branching channel. The magnetohydrodynamic mixed convection flow has been studied by Ishak *et al.,* [27]. Their results show that the magnetic field parameter plays an important role in controlling the boundary layer separation. The numerical study of Selimefendigil *et al.,* [28] discussed the role of magnetohydrodynamic on the forced convection of CuO-water nanofluid flow in a channel with four circular cylinder blocks. The results show that the average Nusselt number increases about 9.34% when the value of Hartmann's number is increased from *Ha*=5 to *Ha*=10. More discussions on the effect of the magnetic field can be found in Ref. [29-36].

Viscous dissipation plays a role as an internal heat generation source in affecting energy transfer, which affects temperature distributions and heat transfer rates. This heat source is caused by the

shearing of fluid layers. In this context, Orhan and Avci [37] numerically studied laminar forced convection with viscous dissipation between two parallel plates. The results found that the variations of the temperature distributions directly depend on the Brinkman number. Increasing the Brinkman number increases the Nusselt number on the heated wall when the movement direction of the upper plate and the main flow are in the same direction, while the opposite is true for the movement of the upper plate in the opposite direction. The heat transfer and entropy generation of a magnetohydrodynamic flow of a viscous incompressible electrically conducting Casson hybrid nanofluid between two infinite parallel non-conducting plates in a rotating frame has been studied by Das *et al.,* [38]. The results show that the minimization in entropy generation is achieved for Casson hybrid nanofluid in comparison with Casson nanofluid. The impacts of viscous dissipation on MHD flow of a fluid in a vertical plate has been studied by Khaled *et al.,* [39]. The results show that the fluid velocity, fluid temperature, the shear stress, and the rate of heat transfer at the wall increase as the Eckert number, Grashof number, thermal conductivity, and the magnetic field increase. Two and three dimensional study of Joule and viscous heating effects of magnetohydrodynamics nanofluid Al2O3-water forced convection in microchannels were numerically studied by Mousavi *et al.,* [40]. They showed that considering Joule and viscous heating effects increases with the enhancement of the magnetic field intensity. Sheikholeslami and Abelman [41] studied the two phase flow of nanofluid in the presence of an axial magnetic field. The effect of viscous dissipation is taken into account. The results show that Nusselt's number is directly related to the aspect ratio and Hartmann's number, but inversely related to Reynolds's number, Schmidt's number, Brownian motion, and Eckert's number. The flow and heat transfer characteristics in three dimensions over a flat surface that is stretched, with the presence of viscous flow has been numerically studied by Mehmood *et al.,* [42]. They concluded that the impact of the Prandtl number on temperature varies depending on the presence of viscous dissipation. When viscous dissipation is present, an increase in the Prandtl number leads to higher temperatures. However, in the absence of viscous dissipation, increasing the Prandtl number results in a decrease in temperature across the channel. The effect of thermal radiation and chemical reaction on MHD free convective heat and mass transfer and the impact of the nanofluid has been investigated on an infinite moving upright plate, Arulmozhi *et al.,* [43]. They showed that the addition of nanoparticles in pure water reduces the velocity and when the chemical reaction parameter increases, the solutal boundary layer thickness decreases. The effects of a magnetic field, with suction and injection, and radiation terms on velocity and thermal slips have been studied by Guled *et al.,* [44]. Their results show that the skin friction increases with higher suction parameter values, magnetic parameters, and the skin friction value decreases as the slip parameter value increases.

According to the literature mentioned above, the entropy generation is one of the most important quantities which interests many researchers. The impacts of addition of nanoparticles and magnetic force in laminar forced convection on the entropy generation rate has been investigated by Atashafrooz *et al.,* [45]. They concluded that the magnitude of the total entropy generation for Al2O3–H2O nanofluid is less compared to CuO–H2O nanofluid. The total entropy generation along the hot channel is reduced significantly with increasing the Lorenz force, and it increases with addition of nanoparticles. These results are discussed in Ref. [46-48].

Many prior studies involving magnetohydrodynamic forced convection flow do not analyze the impact of viscous terms. The novelty of the present study is to investigate numerically laminar MHD forced convection flow of nanoliquid in a rectangular channel with an extended surface, moving top wall and three cylindrical blocks in the presence of a viscous dissipation term. Effects of influential non dimensional parameters (Reynolds number, Hartmann number, Eckert number and

nanoparticles volume fraction) on temperature field distribution, stream function, entropy generation and mean Nusselt number are studied in detail.

2. Problem Configuration and Mathematical Formulation

2.1 Problem Considerations

The present study has been simulated in a two-dimensional rectangular channel with an extended surface crossed by Cu–water nanoliquid and containing three-cylinder hot blocks. The length (L=21H) and the height (2H) of the channel. The length of the extended surface is equal to 3H. A first hot cylinder block of diameter (D=H) is placed in the middle of the channel in the Y direction and the center of the first cylinder in the X direction is placed at 5H. The distance between the cylinders is equal to 5H. The nanoliquid and the top wall move with a constant velocity Uin and Uw respectively, and a cold temperature. A uniform temperature of three-cylinder blocks, extended surface, and bottom wall are imposed. A uniform magnetic flux with uniform intensity B0 acts along the Y-axis, its orientation forms an angle. The 2D schematic of this configuration is described in Figure 1. The thermophysical properties of water (base-liquid) and the copper nanoparticles are presented in Table 1 by Santara *et al*., [50].

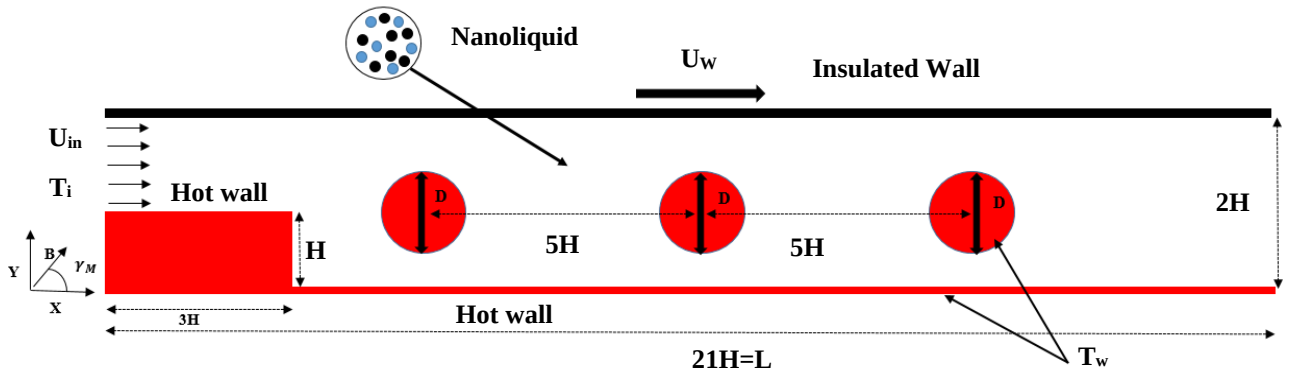

Fig. 1. Schematic of the physique problem

Table 1
Thermo-physical properties of base water and the Cu nanoparticle Santara *et al.,* [50]

Physical properties	Water	Cu
$C_P(J.kg^{-1}.K^{-1})$	4181.8	383.1
$\rho\ (kgm^{-3})$	1000.52	8954
$k(W.m^{-1}.K^{-1})$	0.597	386
$\beta\ (K^{-1})$	21×10^{-5}	51×10^{-6}
$\sigma\ (\Omega m)^{-1}$	0.05	2.7×10^{-8}
$\mu\ \times10^{4}$(kg/ms)	8.55	-

2.2 Governing Equations

In order to write the mathematical model, the following assumptions are used:

i. Steady state flow
ii. The flow is supposed to be incompressible, laminar, and two-dimensional.
iii. The magnetizing force due to the weak magnetic dipole moment is neglected as compared to the Lorentz force.

iv. The mixture of the base fluid and suspended nanoparticles is treated as a single phase with homogeneous effective properties.
v. The fluid is supposed to be Newtonian
vi. The thermo-physical properties are supposed to be constant.
vii. The Joule heating is neglected.
viii. The radiation effects are also neglected.
ix. The nanoparticles are supposed to be of a spherical shape.

When using the aforementioned assumptions, the governing equations can be written as:

$$\frac{\partial u}{\partial x}+\frac{\partial v}{\partial y}=0 \tag{1}$$

$$\rho_{nl}\left[u\frac{\partial u}{\partial x}+v\frac{\partial u}{\partial y}\right]=-\frac{\partial p}{\partial x}+\mu_{nl}\left[\frac{\partial^2 u}{\partial x^2}+\frac{\partial^2 u}{\partial y^2}\right]+\sigma_{nl}B_o^2(v\,sin(\gamma_M)\,cos(\gamma_M)-u\,sin^2(\gamma_M)) \tag{2}$$

$$\rho_{nl}\left[u\frac{\partial v}{\partial x}+v\frac{\partial v}{\partial y}\right]=-\frac{\partial p}{\partial y}+\mu_{nl}\left[\frac{\partial^2 v}{\partial x^2}+\frac{\partial^2 v}{\partial y^2}\right]+\sigma_{nl}B_o^2(v\,sin(\gamma_M)\,cos(\gamma_M)-v\,cos^2(\gamma_M)) \tag{3}$$

$$\rho_{nl}Cp\left[u\frac{\partial T}{\partial x}+v\frac{\partial T}{\partial y}\right]=k_{nl}\left(\frac{\partial^2 T}{\partial x^2}+\frac{\partial^2 T}{\partial y^2}\right)+\Phi \tag{4}$$

The equations related to the non-dimensioning of governing equations for laminar and MHD forced nanoliquid flow are described as follows:

$$X=\frac{x}{H},Y=\frac{y}{H},U=\frac{u}{u_{in}},V=\frac{v}{u_{in}}Pr=\frac{v_{nl}}{\alpha_{nl}},\theta=\frac{T-T_{in}}{T_w-T_{in}},Re=\frac{u_{in}D_h}{v_{nl}},P=\frac{p}{u_{in}^2},Ha=HB_o\sqrt{\frac{\sigma_{nl}}{\mu_{nl}}},Ec=\frac{u_w^2}{Cp_{nl}(T_{in}-T_w)} \tag{5}$$

By substituting this dimensionless variable in Eq. (1–4), governing equations in the dimensionless state can be written as follows Karimipour *et al.,* [21]:

$$\frac{\partial U}{\partial X}+\frac{\partial V}{\partial Y}=0 \tag{6}$$

$$U\frac{\partial U}{\partial X}+V\frac{\partial U}{\partial Y}=-\frac{\partial P}{\partial X}+\frac{1}{Re\left[\frac{\partial^2 U}{\partial X^2}+\frac{\partial^2 U}{\partial Y^2}\right]\frac{Ha^2}{Re\,sin(_M\,cos(_M\,sin^2(_M}} \tag{7}$$

$$U\frac{\partial V}{\partial X}+V\frac{\partial V}{\partial Y}=-\frac{\partial P}{\partial Y}+\frac{1}{Re\left[\frac{\partial^2 V}{\partial X^2}+\frac{\partial^2 V}{\partial Y^2}\right]\frac{Ha^2}{Re\,sin(_M\,cos(_M\,cos^2(_M}} \tag{8}$$

$$U\frac{\partial \theta}{\partial X}+V\frac{\partial \theta}{\partial Y}=\frac{1}{Pr.Re\left(\frac{\partial^2 \theta}{\partial X^2}+\frac{\partial^2 \theta}{\partial Y^2}\right)\frac{Ec}{Re\left(\frac{\partial U}{\partial Y}+\frac{\partial V}{\partial X}\right)^2}} \tag{9}$$

The boundary conditions of this problem are given by Miri *et al.,* [11] in Table 2:

Table 2
Boundary conditions

	Velocity boundary conditions	Temperature boundary conditions
At the inlet of channel	$U = 1; V = 0$	$\theta = 0$
At the outlet of channel	$\frac{\partial U}{\partial X} = \frac{\partial V}{\partial X} = 0$	$\frac{\partial \theta}{\partial X} = 0$
At the downstream bottom wall of channel	$U = 0; V = 0$	$\theta = 1$
At the top wall of channel	$U = 1; V = 0$	$\theta = 0$
At the hot cylinder blocks	$U = 0; V = 0$	$\theta = 1$

2.3 Nanoliquid Properties

The heat capacitance, density, thermal diffusivity, thermal conductivity, viscosity and electrical conductivity of the nanoliquid are given in Table 3, Mliki *et al.,[*12]:

Table 3
Nanoliquid properties, Mliki *et al.,* [12]

Properties	Mathematical formulation
The heat capacitance	$(\rho C_P)_{nl} = (1-\phi)(\rho C_P)_l + \phi(\rho C_P)_p$
Density	$\rho_{nl} = (1-\phi)\rho_l + \phi\rho_p$
Thermal diffusivity	$\alpha_{nl} = k_{nl}/(\rho C_P)_{nl}$
Thermal conductivity	$k_{nl} = k_l \frac{k_p + 2k_l - 2\phi(k_l - k_p)}{k_p + 2k_l + \phi(k_l - k_p)}$
The effective viscosity	$\mu_{nl} = \frac{\mu_l}{(1-\phi)^{2.5}}$
The electrical conductivity	$\sigma_{nl} = \sigma_l \left[1 + \frac{3(\sigma_s/\sigma_l - 1)\phi}{(\sigma_s/\sigma_l + 2) - (\sigma_s/\sigma_l - 1)\phi}\right]$

2.4 Parameters of Engineering Interest

The convective heat transfer is described using Nusselt number along the bottom wall, the local and average Nusselt number are expressed as follows:

$$Nu = -\frac{k_{nl}}{k_l}\left(\frac{\partial \theta}{\partial Y}\right)\Big|_{Y=0} \tag{10}$$

$$Nu_{avg} = \frac{1}{L}\int_0^L Nu.\, dX \tag{11}$$

The relationships between the stream function and velocity components can be calculated by:

$$U = \frac{\partial \psi}{\partial Y} \text{ and } V = -\frac{\partial \psi}{\partial X} \tag{12}$$

It can be written in a single equation:

$$\frac{\partial^2 \psi}{\partial X^2} + \frac{\partial^2 \psi}{\partial Y^2} = \frac{\partial U}{\partial Y} - \frac{\partial V}{\partial X} \tag{13}$$

The local dimensionless entropy generation is the result of the sum of the irreversible heat transfer, the fluid friction, and the magnetic field.

$$S_{gen} = S_{gen,h} + S_{gen,v} + S_{gen,M} \tag{14}$$

The first term relative to the heat transfer irreversibility:

$$S_{gen,h} = \frac{k_{nl}}{k_l}\left[\left(\frac{\partial\theta}{\partial X}\right)^2 + \left(\frac{\partial\theta}{\partial Y}\right)^2\right] \tag{15}$$

The second term corresponds to fluid friction irreversibility:

$$S_{gen,v} = \chi\frac{\mu_{nl}}{\mu_l}\left\{2\left[\left(\frac{\partial U}{\partial X}\right)^2 + \left(\frac{\partial V}{\partial Y}\right)^2\right] + \left[\left(\frac{\partial U}{\partial Y}\right) + \left(\frac{\partial V}{\partial X}\right)\right]^2\right\} \tag{16}$$

The last term associated with the magnetic field irreversibility:

$$S_{gen,M} = \chi \times Ha^2 \times \left[(1-\phi) + \phi\frac{\rho_s}{\rho_l}\right] \times [U\,sin(\gamma_M) - V\,cos(\gamma_M)]^2 \tag{17}$$

Whereχrepresents the irreversibility factor:

$$\chi = \frac{\mu_{nl}T_{in}U_{in}^2}{k_{nl}(T_w - T_{in})^2} \tag{18}$$

Bejan number (Be) which is important while discussing entropy generation, is defined as the ratio of entropy generation due to heat transfer and total entropy generation:

$$Be_{Local} = \frac{S_{gen,h}}{S_{gen}} \tag{19}$$

The total entropy generation (S_{gen}) and the Bejan number (Be) are calculated by the integration over the whole domain Ω as:

$$S_{gen} = \iint_{\Omega} S_{gen}\ dXdY$$
And,
$$Be = \iint_{\Omega} Be_{Local}\ dXdY \tag{20}$$

3. LBM Method

The lattice Boltzmann approach (LBM) has been used in this work. To simulate flow and heat transfer of nanoliquid in a 2D backward facing step. The D2Q9 model was selected as shown in Figure 2 (a) for the dynamic field and with the D2Q4 for the thermal field Figure 2 (b).

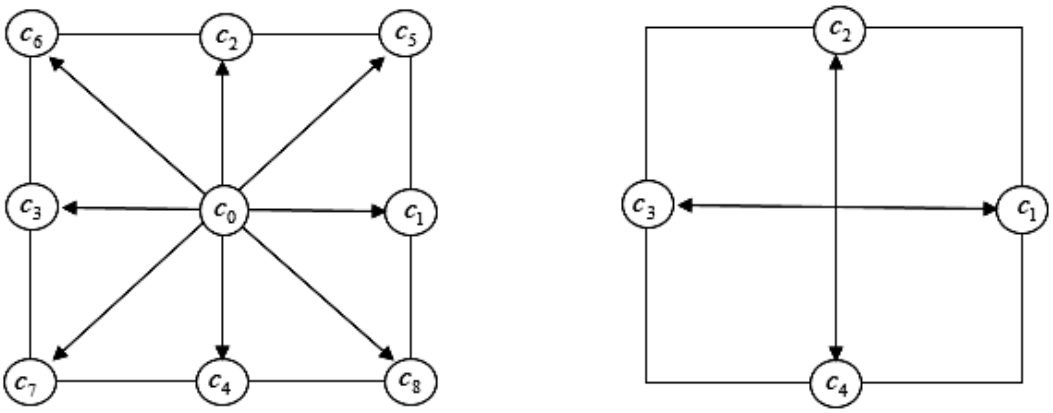

(a) (b)

Fig. 2. D2Q9- D2Q4 models: for the (a) velocity field and (b) temperature field

The Lattice Boltzmann Equation (LBE) with external term force is solved using the BGK approximation.

For the dynamic field:

$$f_k(x + c_k\Delta t, t + \Delta t) = f_k(x,t) + \frac{\Delta t}{\tau_v}\left[f_k^{eq}(x,t) - f_k(x,t)\right] + \Delta t c_k F_k \tag{21}$$

Where Δt, τ, c_k, F_k and f_k^{eq} denotes respectively the lattice time step, the relaxation time, the discrete lattice velocity in direction (i), the external force in direction of lattice velocity, and the equilibrium distribution function.

For the temperature field:

$$g_k(x + c_k\Delta t, t + \Delta t) = g_k(x,t) + \frac{\Delta t}{\tau_g}\left[g_k^{eq}(x,t) - g_k(x,t)\right] \tag{22}$$

τ_v and τ_g are the relaxation times for the flow and temperature fields, f_k^{eq} and g_k^{eq} are the equilibrium distribution functions given for the D2Q9-D2Q4 models respectively as:

$$f_k^{eq} = \rho\omega_k\left[1 + 3\frac{c_k.u_i}{c^2} + \frac{9(c_k.u_i)^2}{2c^4} - \frac{3{u_i}^2}{2c^2}\right] \tag{23}$$

$$g_k^{eq} = \theta\omega_k[1 + 2c_k.u_i] \tag{24}$$

For the D2Q9, the weighting factors and the discrete particle velocity vectors are defined as follows:

$$\begin{pmatrix}\omega_k\\ c_{k,x}\\ c_{k,y}\end{pmatrix} = \begin{pmatrix}\frac{4}{9}, \frac{1}{9}, \frac{1}{9}, \frac{1}{9}, \frac{1}{9}, \frac{1}{36}, \frac{1}{36}, \frac{1}{36}, \frac{1}{36}\\ 0, \ 1, \ 0, -1, 0, \ 1, \ -1, \ -1, \ 1\\ 0, \ 0, \ 1, \ 0, -1, \ 1, \ \ 1, \ -1, -1\end{pmatrix} \tag{25}$$

The macroscopic quantities are calculated by the following equations:

$$\rho = \sum_{k=0-8} f_k \tag{26}$$

$$\rho u = \sum_{k=0-8} f_k\, c_k + \Delta t F \tag{27}$$

$$\theta = \sum_{k=0-4} g_k \tag{28}$$

The unknown distribution functions are calculated by the following relations in Table 4:

Table 4
Boundary conditions for *f* and g distribution function

	Velocity boundary conditions	Temperature boundary conditions
At the inlet	$\rho_{in} = \frac{f_0 + f_2 + f_4 + 2(f_3 + f_6 + f_7)}{1 - u_{inlet}}$ $f_1 = f_3 + \frac{2}{3}\rho u_{inlet}$ $f_5 = f_7 + \frac{1}{2}(f_4 - f_2) + \frac{1}{6}\rho u_{inlet}$ $f_8 = f_6 - \frac{1}{2}(f_4 - f_2) + \frac{1}{6}\rho u_{inlet}$	$g_1 = \theta\big(\omega(1) + \omega(3)\big) - g_3$ $g_5 = \theta\big(\omega(5) + \omega(7)\big) - g_7$ $g_8 = \theta\big(\omega(6) + \omega(8)\big) - g_6$
At the outlet of the channel	$f_3(n,j) = 2f_3(n-1,j) - f_3(n-2,j)$ $f_6(n,j) = 2f_6(n-1,j) - f_6(n-2,j)$ $f_7(n,j) = 2f_7(n-1,j) - f_7(n-2,j)$	$g_3(n,j() g_3(n-1,j() g_3(n-2,j()))$ $g_6(n,j() g_6(n-1,j() g_6(n-2,j()))$ $g_7(n,j() g_7(n-1,j() g_7(n-2,j()))$
At the top boundary	$f_4(i,m) = f_2(i,m)$ $f_7(i,m) = f_5(i,m)$ $f_8(i,m) = f_6(i,m)$	$g_4(i,m) = g_4(i,m-1)$ $g_7(i,m) = g_7(i,m-1)$ $g_8(i,m) = g_8(i,m-1)$
At the heated part of the walls		$g_4(i,m) = \theta\big(\omega(4) + \omega(2)\big) - g_2(i,m)$ $g_7(i,m) = \theta\big(\omega(7) + \omega(5)\big) - g_5(i,m)$ $g_8(i,m) = \theta\big(\omega(8) + \omega(6)\big) - g_6(i,m)$

4. Physical Interpretations and Discussion

4.1 Independency from Iteration Number

Table 5 indicates the demanded iterations number for results independency from gridding. The selected iteration number has been studied from 1000 to 200000 for the nanoliquid in Reynolds number of 100. In this investigation, the independence of flow and heat transfer parameters was intended. For the chosen iteration number, the average Nusselt numbers on the bottom wall have been compared with different iteration numbers. According to the changes of parameters in the chosen iteration number, it is observed that the iteration number of 50000, in comparison with the lower iteration number, has more accurate results. In this study, this iteration number has been used as an acceptable iteration number in the simulation of the numerical solving domain of heat transfer and flow.

Table 5
Average Nusselt number on the bottom wall for different iteration numbers

Iteration number	1000	5000	10000	50000	100000	200000
Average Nusselt number	52.870	26.228	16.127	13.338	13.339	13.339

4.2 Validation of the Numerical Code

In order to verify the accuracy of the present results, the local Nusselt number values have been compared with those reported by Alashafrooz *et al.,* [49] and Santara *et al.,* [50]. These comparisons show excellent agreement (Figure 3 and Figure 4) and Table 6.

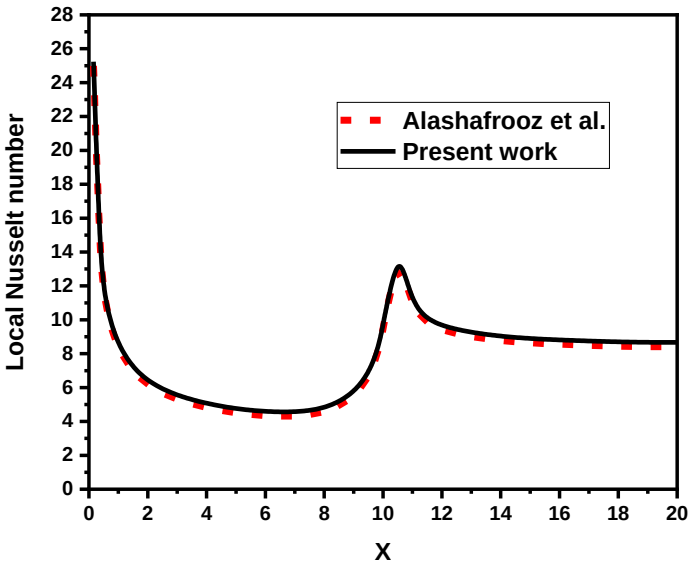

Fig. 3. Local Nusselt number variation compared to those of Alashafrooz *et al.,*[49] for *Re*=400; ϕ=0.04

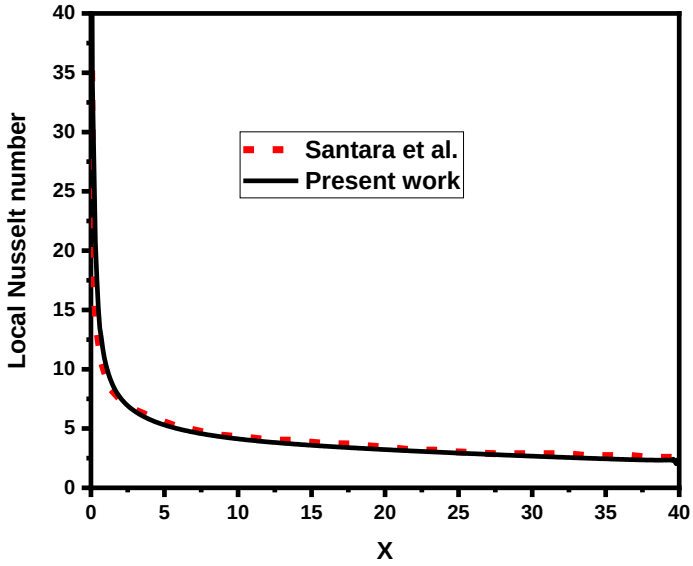

Fig. 4. Comparison of the Nusselt number distribution along the bottom wall with results obtained by Santara *et al.,* [50] for *Re*=100; ϕ=0.025

Table 6
Comparison of average Nusselt number along the bottom wall with results obtained by Ferhi *et al.,* [51] for Re=10; ϕ=0;

	Nu_{avg}	
Grid size	**This works**	**Ferhi *et al.,* [51]**
100×25	9.800	9.850
200×50	9.905	9.900
400×100	9.945	9.940

4.3 Independency from Grid

The corresponding values of the average Nusselt number along the bottom wall are calculated and tabulated for several different grids in Table 7. According to this table, the numerical results are almost the same for meshes smaller than 840×80, so that there is no significant change in the results. Thus, an 840×80 mesh was selected to implement the code. All computations in this research are performed using a computer program written in Fortran.

Table 7
Grid independence test results for Re=50; ϕ=0.02; Ec=0.5; Ha=0; γM=0

Grid size	Nu_{avg}	Percentage of the difference
105×10	6.123	—
210×20	6.421	4.86%
420×40	6.569	2.30%
840×80	6.571	0.03%
1680×160	6.572	0.015%

4.4 Effects of Reynolds Number

In this section, we are interested in the effects of Reynolds numbers. Figure 5 shows the influence of Reynolds numbers on the streamlines and isotherms contours for Ha=0; ϕ=0.02; Ec=0.5. As can be seen, with the increase in Reynolds numbers, the length of the recirculation zone behind the step is increasing and the flow of nanoliquid becomes faster. An increase in the Reynolds number causes a reduction in the thickness of the thermal boundary layer, leading to a higher level of compression observed in the streamlines. The maximum and the minimum values of the stream function are equal to (Ψmax=3007.96; Ψmin=-142.716) and are calculated for Re=200. On the other hand, the isotherms' contours are more clustered along the bottom hot wall. As a result, the flow of nanoliquid near the cold wall exhibits greater flexibility. It can be concluded that the external inertia forces dominate, which leads to heat transfer enhancement.

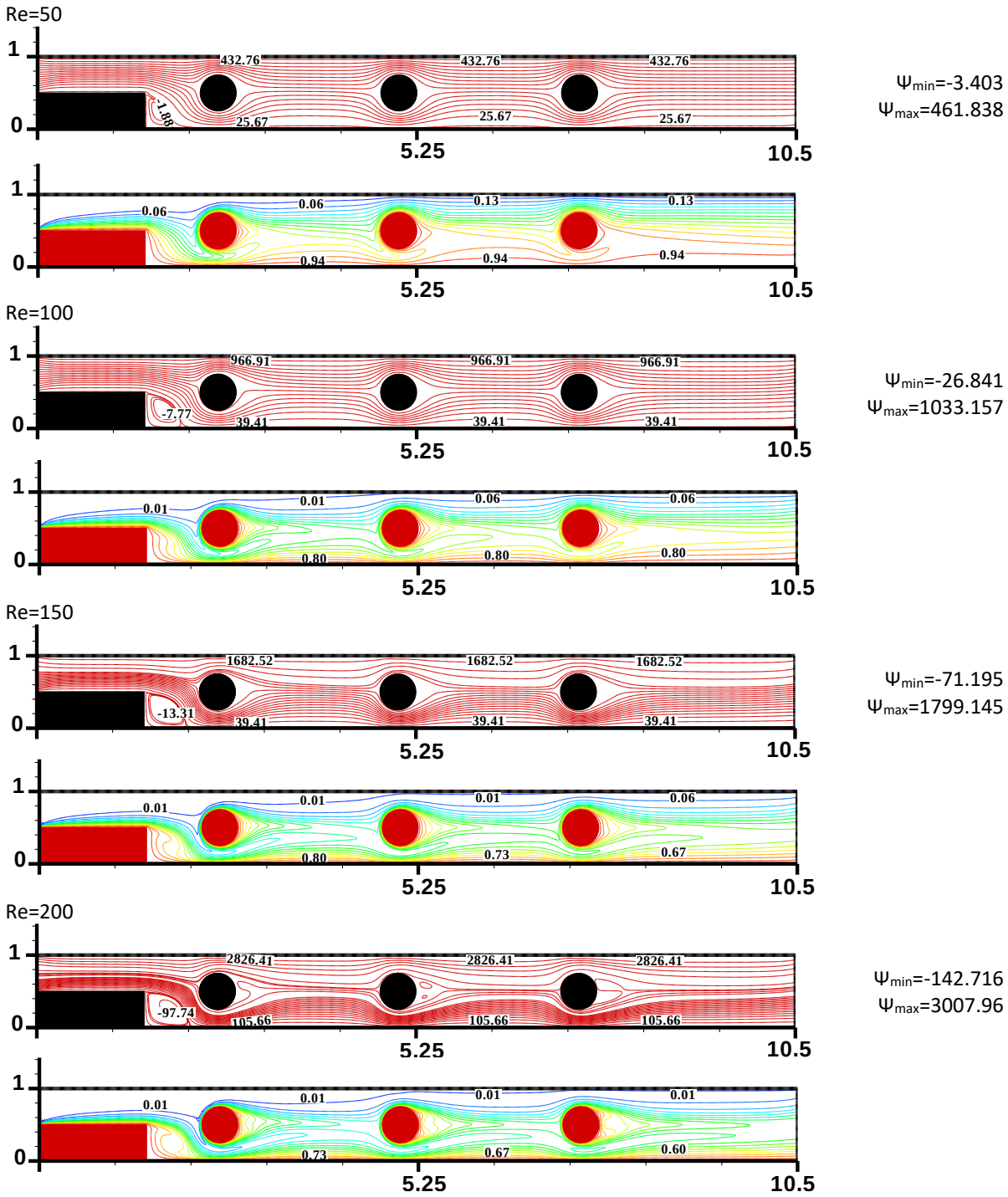

Fig. 5. Streamlines and isotherms contours for different Reynolds number at Ha=0; ϕ=0.02; Ec=0.5

For the same parameters, the average Nusselt number (*Nuavg*) on the bottom hot wall in terms of Reynolds number is shown in Figure 6. The average Nusselt is an increasing function of Reynolds number for all values of Hartmann number. This means that the higher velocity of the nanoliquid leads to increased forced convection and hence the value of *Nuavg*. This can be directly explained by the growth of the inertia forces.

Also, the variation of Nulocal on the bottom hot wall for Re=50-100-150-200; Ha=0; ϕ=0.02; Ec=0.5 is shown in Figure 7. Three picks have been observed in the curve of the local Nusselt number on the bottom wall. These picks are due to the presence of three-cylinder hot blocks, the presence of the recirculation zone behind the extended surface increases the flow of nanoliquid. At Reynolds

number equal to 200, the first, second, and third picks had maximum local Nusselt numbers (Nulocal=81.624; Nulocal=64.306; Nulocal=61.464) respectively. As a result, increasing the Reynolds number leads to increasing the convection mechanism results, which in turn results in higher heat transfer coefficients in terms of local Nusselt numbers. It can be concluded that the inertial forces dominate over the viscous forces.

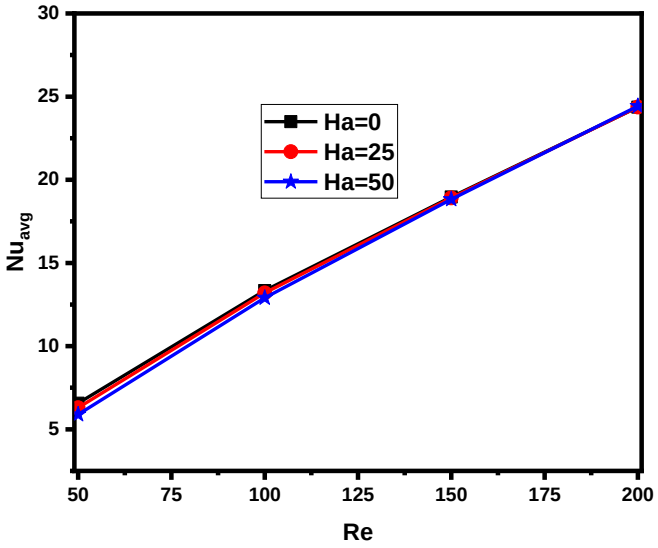

Fig. 6. Variation of Nu_{avg} in function of Re for Ha=0-25-50; ϕ=0.02; Ec=0.5

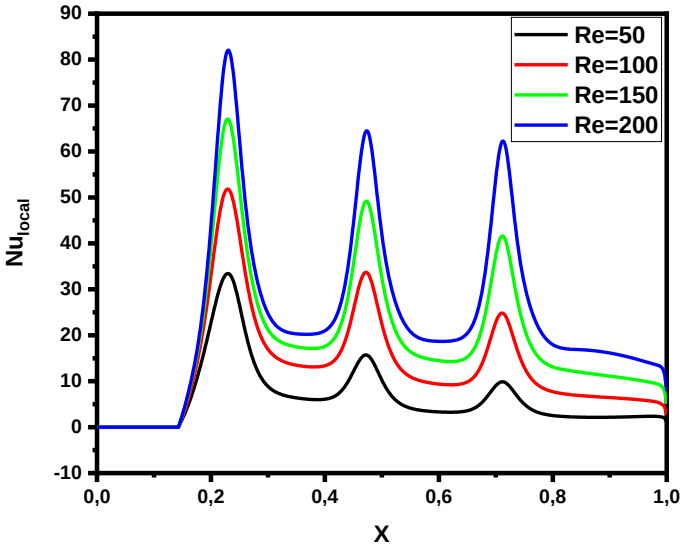

Fig. 7. Variation of Nu_{local} for Re=50-100-150-200; Ha=0; ϕ=0.02; Ec=0.5

Figure 8 shows the distribution of X-component velocity at X=0.5 for Re=50-100-150-200; Ha=0; ϕ=0.02; Ec=0.5. The increase of Reynolds number allows us to increase the velocity component in X direction. This shows that the velocity of the flow depends directly on the Reynolds number. Also, the presence of a recirculation zone behind the extended surface can be observed by the negative values of the axial velocity component just for Re=150-200. This influence is due to enhancement of the inertia forces. It demonstrates the domination of the convective mode of nanoliquid. On the other hand, Figure 9 shows the variation in temperature profile at X=0.5. It is evident from the

observation that as the value of the Reynolds number increases, the temperature profile in X direction decreases. These results confirm that the heat transfer rate is increased by the enhancement of Reynolds number. It can be explained by the fact that the motion of nanoliquid becomes faster, which enhances the convective heat transfer coefficient and reduces the conductive mode.

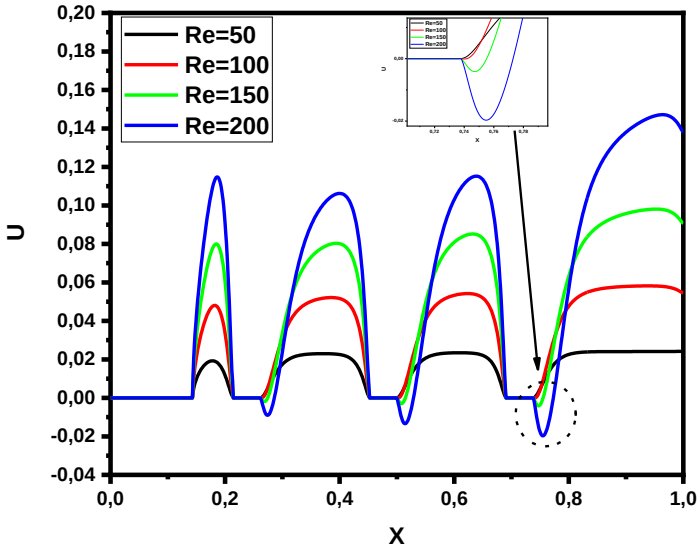

Fig. 8. Variation of U (X;0.5) for Re=50-100-150-200; Ha=0; ϕ=0.02; Ec=0.5

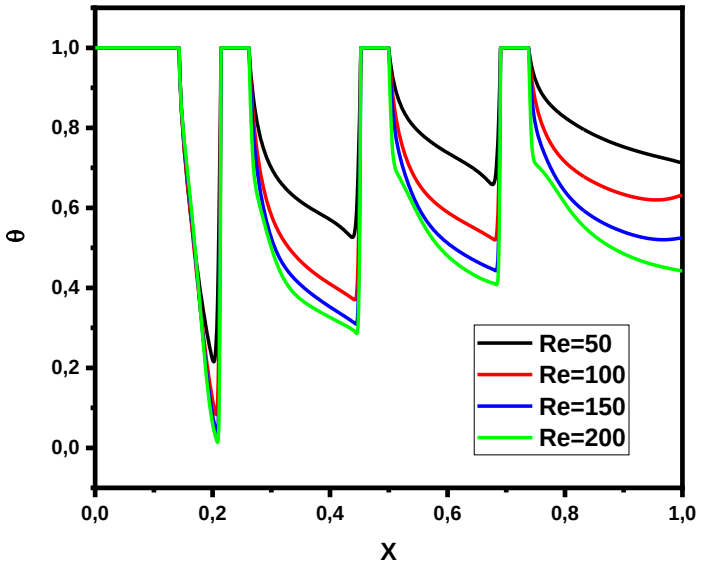

Fig. 9. Variation ofθ (X;0.5) for Re=50-100-150-200; Ha=0; ϕ=0.02; Ec=0.5

Figure 10 represents the influence of the Reynolds number (Re) on the total entropy generation (Sgen) and the Bejan number (Be) for Ha=0-25-50; ϕ=0.02; Ec=0.5, respectively. It is clear that the increase in (Re) enhances the total entropy generation. The increase in total entropy generation signifies a rise in overall irreversibility. This impact indicates that more energy is being dissipated in nanoliquid. On the contrary, the curve of Bejan numbers decreased. These performances are due to enhanced terms of entropy generation due to heat transfer and fluid friction.

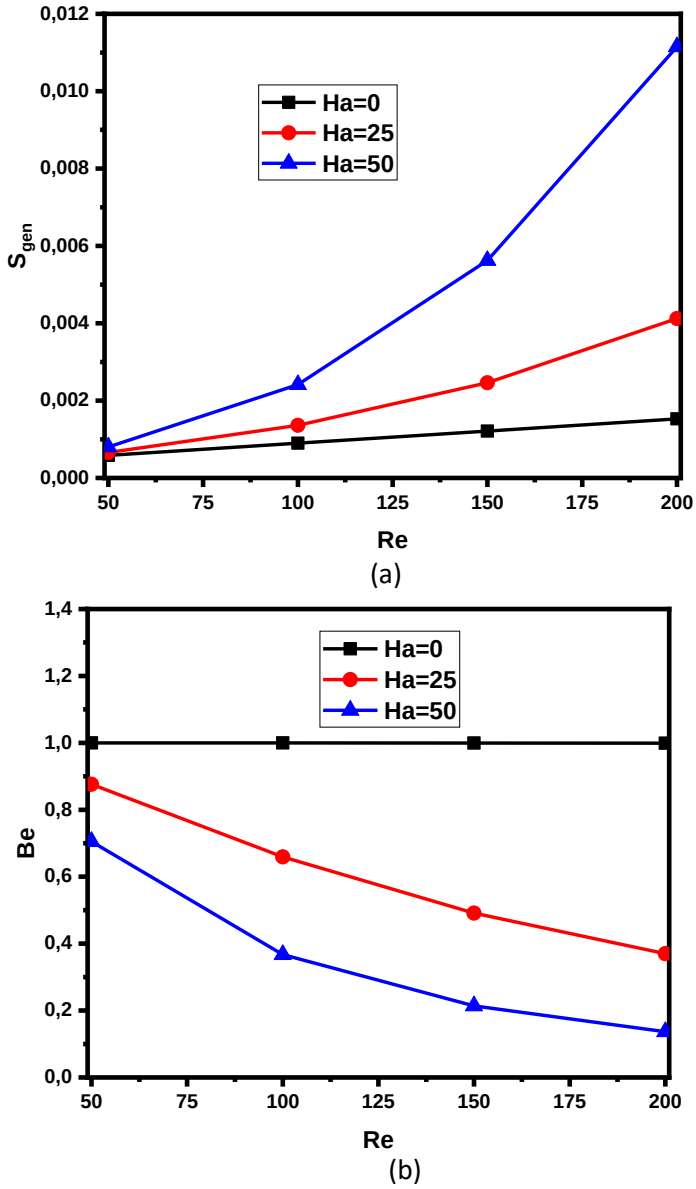

Fig. 10. Variation of (a) the total entropy generation and (b) the Bejan number in function of Re for Ha=0-25-50; ϕ=0.02; Ec=0.5

4.5 Effect of Hartmann Number

Figure 11 illustrates the influence of Hartmann number on streamlines and isotherm contours for Re=100; ϕ=0.02; Ec=0.5. As can be seen by increasing the Hartmann number, a recirculation zone disappears behind the extended surface. The size of these recirculation zones decreases with the Hartmann number. As the magnetic field is applied, the recirculation cells are more compressed, which is a sign of augmented nanoliquid velocity in the channel. Moreover, the maximum value of the stream function is enhanced by the magnetic field. The maximum and the minimum values of the stream function (Ψmax=1060.284; Ψmin=-1.684) are calculated for Ha=50, respectively. The physical reason for this phenomenon is the interaction of external Lorentz force along with the buoyancy and shear driven flow has a tendency to speed up the movement of the nanoliquid within the channel.

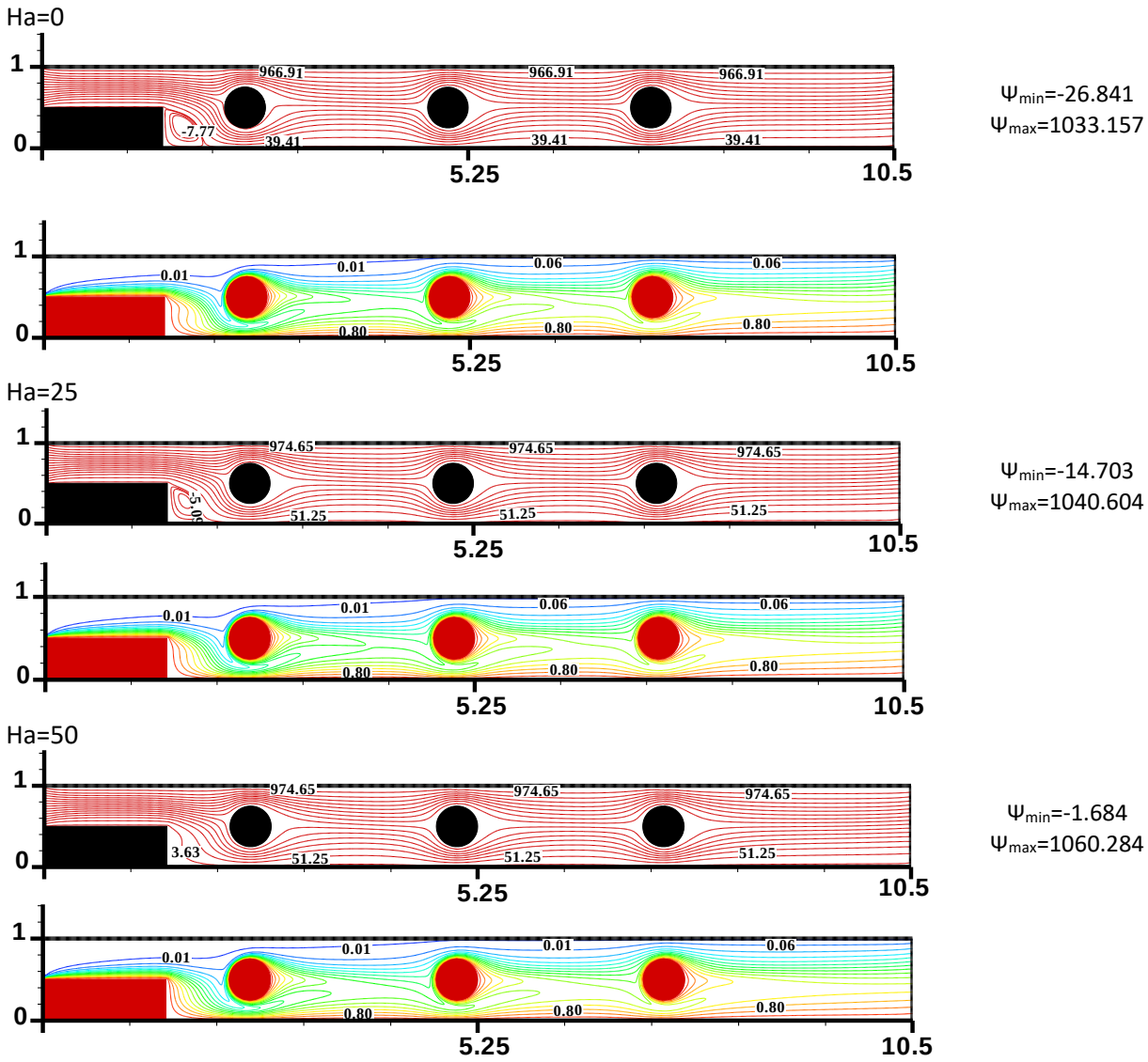

Fig. 11. Streamlines and isotherms contours for different Hartmann number at Re=100; ϕ=0.02; Ec=0.5

Figure 12 presents the variation of the average Nusselt number (*Nuavg*) in function of Hartmann number for Re=50-100-200; ϕ=0.02; Ec=0.5. For all values of Reynolds number, the average Nusselt number slightly decreased with the rise of the Hartmann number. As a result, the magnetic field reduces the average Nusselt number. The reason for this behavior is that the flow of nanoliquid is steady at higher Hartmann number values. For more details, the local Nusselt number distribution is presented in Figure 13 for the same conditions. From this figure, it can be seen that the presence of the external magnetic field decreases the local Nusselt number. The influence of the Hartmann number is remarkable when the conductive mode dominates. The negative impact of the volumetric force is clearly observed. Also, the presence of a magnetic field causes a decrease in the three peaks in this curve. At Hartmann number numbers equal to 50, the first, second, and third picks had maximum values equal to (Nulocal=43.299; Nulocal=29.523; Nulocal=22.018) respectively.

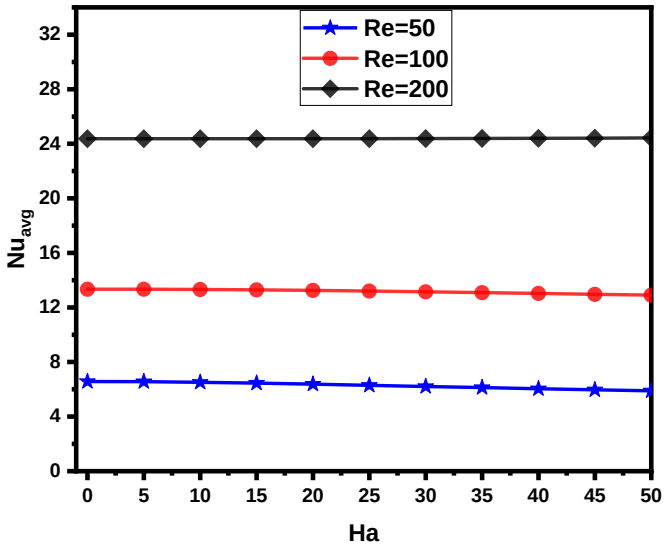

Fig. 12. Variation of Nu_{avg} in function of Hartmann number for Re=50-100-200; ϕ=0.02; Ec=0.5

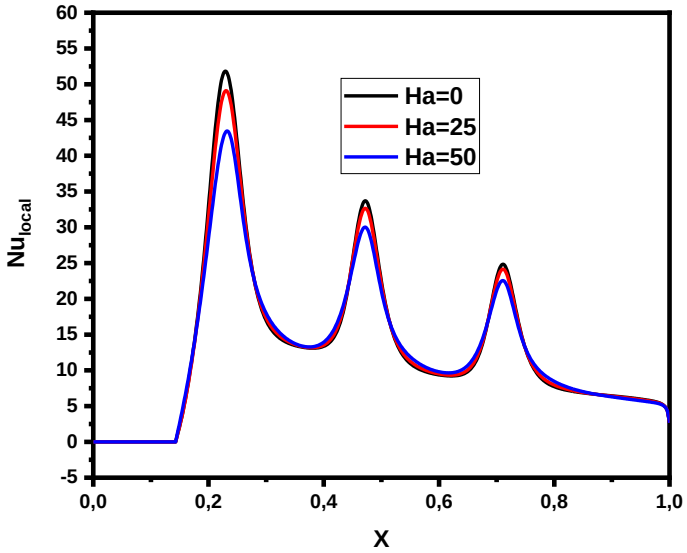

Fig. 13. Variation of Nu_{local} for Re=100; Ha=0-25-50; ϕ=0.02; Ec=0.5

Figure 14 presents the distribution of the velocity component profile in X- direction at X=0.5 for Re=100; Ha=0-25-50; ϕ=0.02; Ec=0.5. The numerical results show that the velocity component profile in X-direction is reduced when the Hartmann number is increased. These effects are observed when the nanoliquid moves between the hot blocks, which means the impact of the external magnetic force is detected when the nanoliquid moves more smoothly. Similarly, the same influence is detected on the temperature profile in X direction at X=0.5 in Figure 15 but in a lighter way. The opposite effects of the Lorentz force and inertia forces on the flow of cu-water are detected. It can be concluded that the Lorentz force retards the velocity and temperature of the flow of nanoliquid.

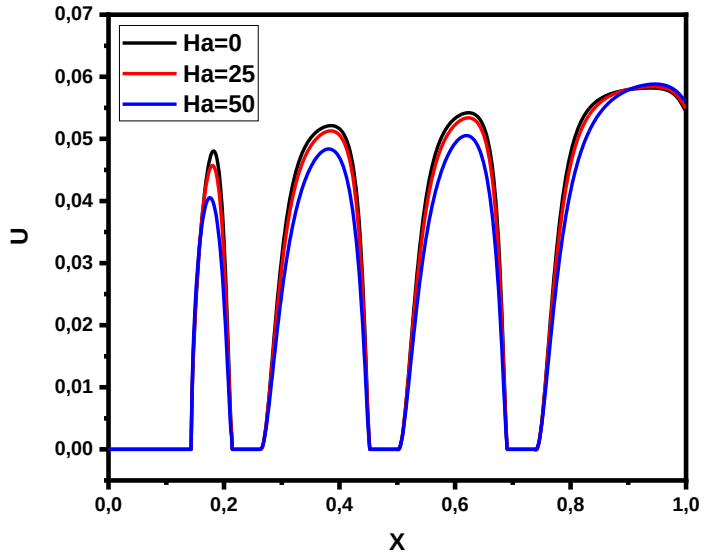

Fig. 14. Variation of U (X;0.5) for Re=100; Ha=0-25-50; ϕ=0.02; Ec=0.5

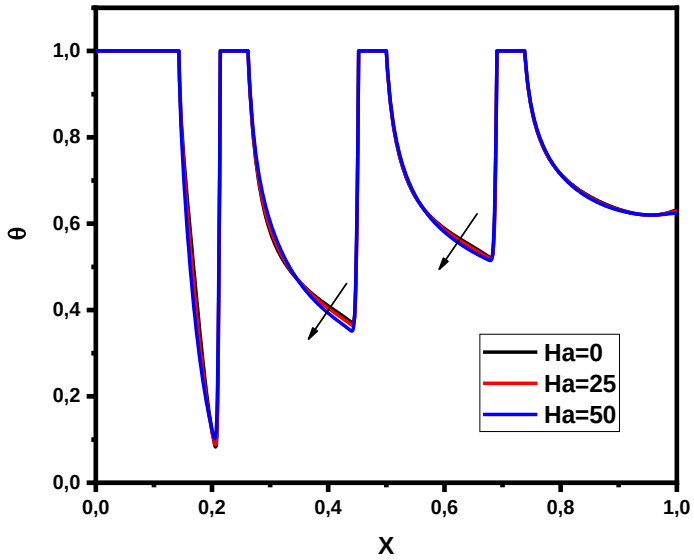

Fig. 15. Variation ofθ (X;0.5) for Re=100; Ha=0-25-50; ϕ=0.02; Ec=0.5

Figure 16 shows the effect of Hartmann number (Ha) on the total entropy generation (Sgen) and the Bejan number (Be) for Re=50-100-150-200; ϕ=0.02; Ec=0.5. It is found that the total entropy generation (Sgen) is an increasing function with Hartmann number, also the influence of Ha is more detecting at high values of (Re). It can be concluded that the magnetic field increases the irreversibility of nanoliquid. On the other hand, the curve of Bejan numbers is decreasing. Physically, the magnetic field irreversibility is more dominating than the fluid friction irreversibility.

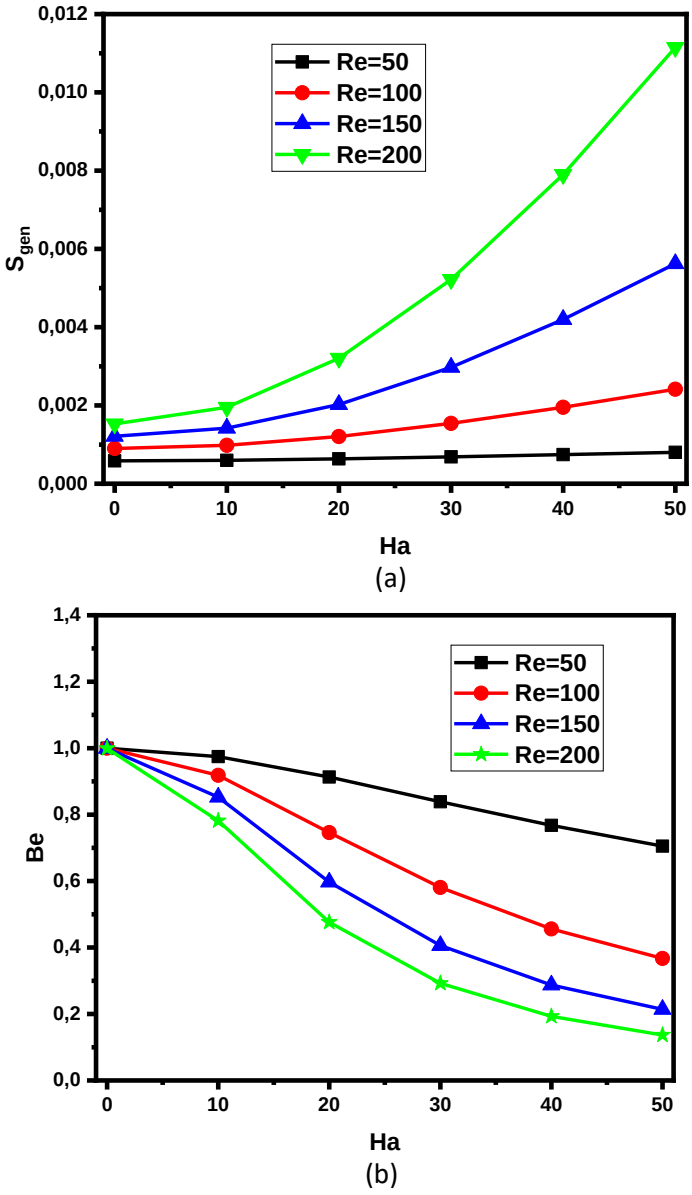

Fig. 16. Variation of the total entropy generation (a) and the Bejan number (b) in function of Ha for Re=50-100-150-200; ϕ=0.02; Ec=0.5

4.6 Effects of Eckert Number

Figure 17 depicts the effect of Eckert numbers on the streamlines and isotherms contours for Ha=50; Re=50; ϕ=0.02. The streamlines become closer to each other. The maximum and the minimum values of the stream function are detected for Ec=1.0 which are equal to (Ψmax=475.65; Ψmin=-1.65×10-4) respectively. The isothermal contour is compressed in y-direction and becomes stretched in X-direction with an existing increase in the viscous dissipation. This influence of Eckert numbers can clearly be seen when the isothermal lines approach the three-cylinder hot blocks. This result indicates that the motion of the upper wall gives a positive effect on the heat transfer rate of the nanoliquid.

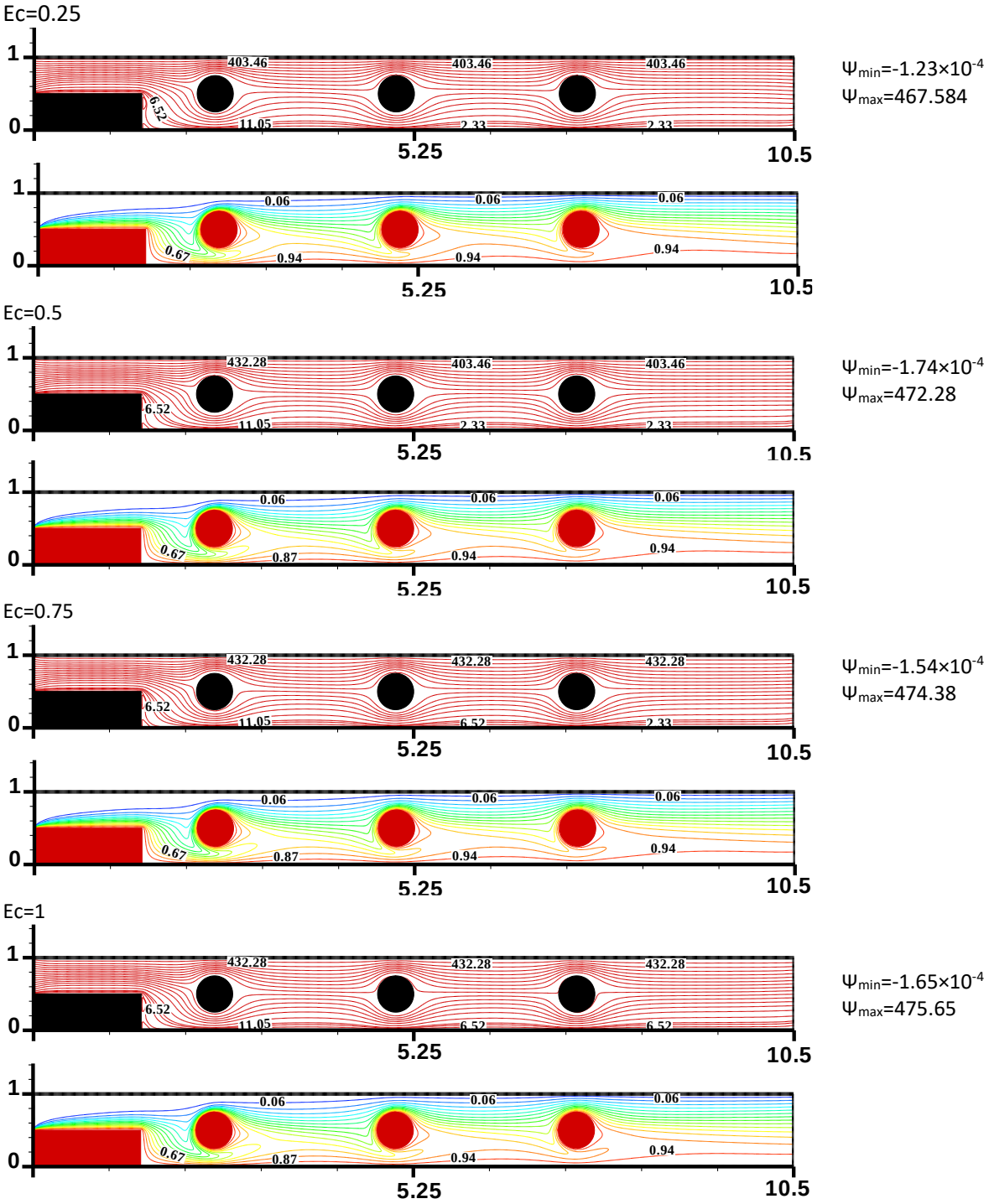

Fig. 17. Streamlines and isotherms contours for different Eckert number at Ha=50; Re=50; ϕ=0.02

Figure 18 illustrates the variations of the average Nusselt number depending on the Eckert number for Re=50-100-150-200; Ha=50; ϕ=0.02. The increase in values of the Eckert number causes an increase in the average Nusselt number. The effect of Eckert's number is more noticeable for Re =50. As a result, the heat transfer rate is enhanced with the viscous dissipation term. A low Eckert number implies that the thermal energy dominates over the kinetic energy, while a high Eckert number indicates the opposite.

Figure 19 illustrates the variations of the average Nusselt number in function of Eckert number for Re=50; Ha=0-25-50; ϕ=0.02. The numerical results indicated that the average Nusselt number

increased as the Eckert number increased for all values of Hartmann numbers. Moreover, more influence of viscous dissipation on the heat transfer is detected in the presence of the magnetic force. This is due to enhancement of the temperature gradient at the hot wall. These effects are confirmed by the curve of local Nusselt numbers present in Figure 20. It means that the kinetic energy increases. This can be explained by the increase in the translation velocity of the upper wall.

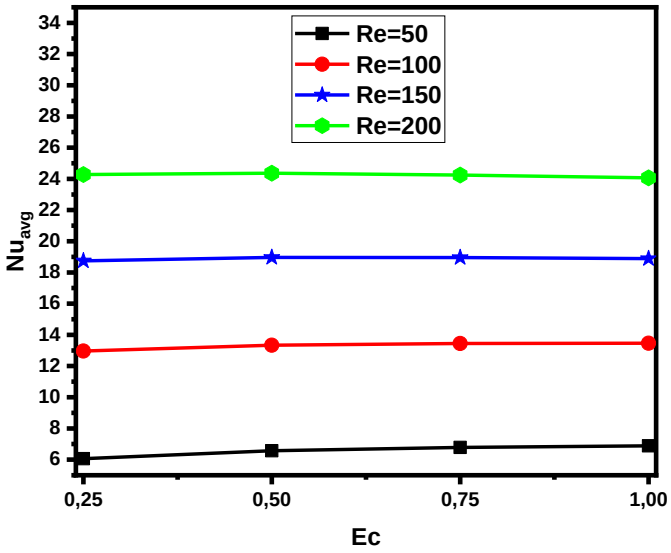

Fig. 18. Variation of Nu_{avg} in function of Eckert number for Re=50-100-150-200; Ha=0; ϕ=0.02

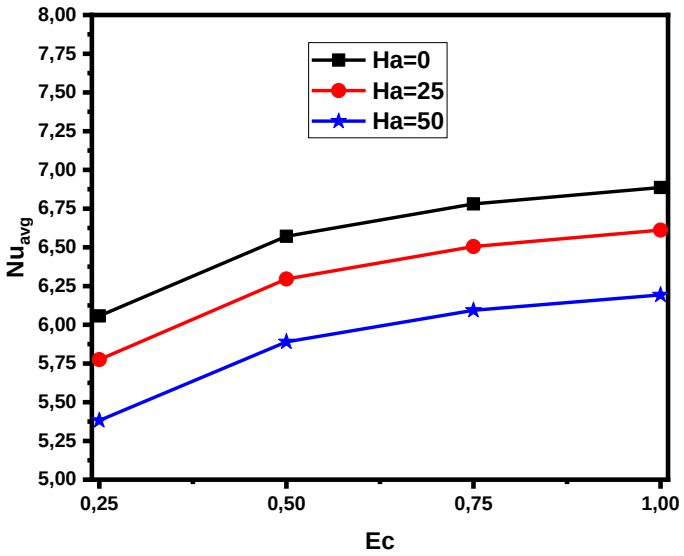

Fig. 19. Variation of Nu_{avg} in function of Eckert number for Re=50; Ha=0-25-50; ϕ=0.02

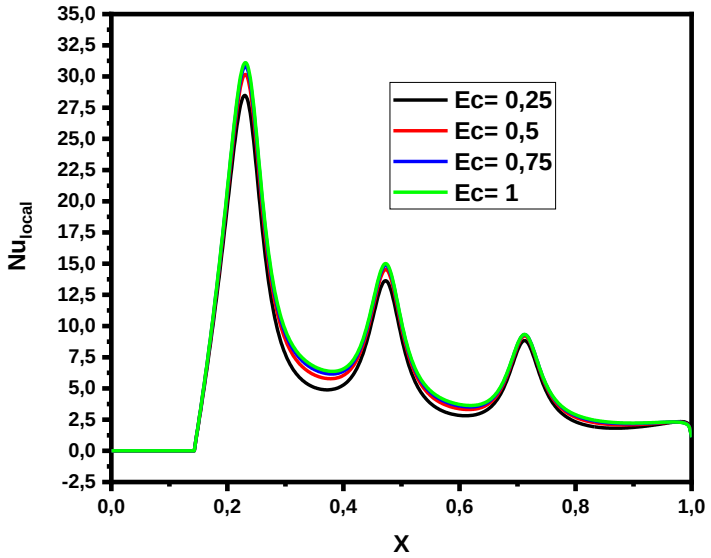

Fig. 20. Variation of Nu_{local} for different Eckert number at Re=50; Ha=25; ϕ=0.02

Figure 21 and Figure 22 show the distribution of the component of velocity and the temperature profile in X-direction (X=0.5) for various values of the Eckert number and Re=50; Ha=25; ϕ=0.02. The increase in values of the Eckert number causes an increase in the velocity profile. On the other hand, the temperature profile decreases. This result indicates that the movement of the top wall has the same influence of the inertial forces. The main cause of this influence is the increase in viscous dissipation.

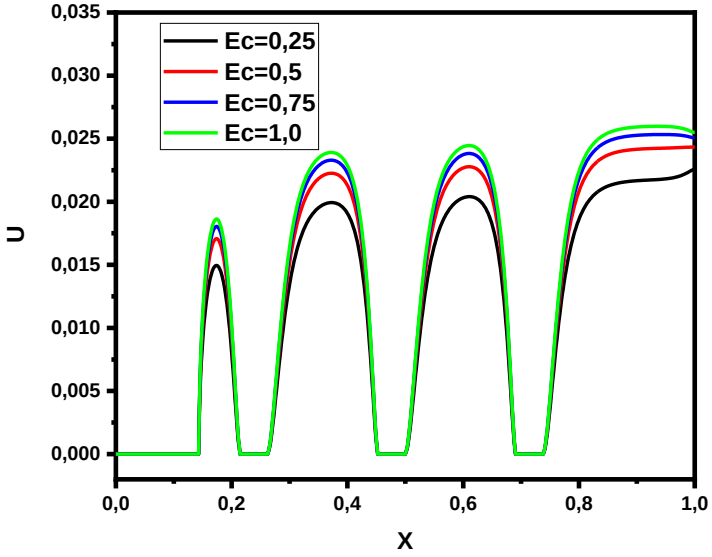

Fig. 21. Variation of U (X;0.5) for different Eckert number at Re=50; Ha=25; ϕ=0.02

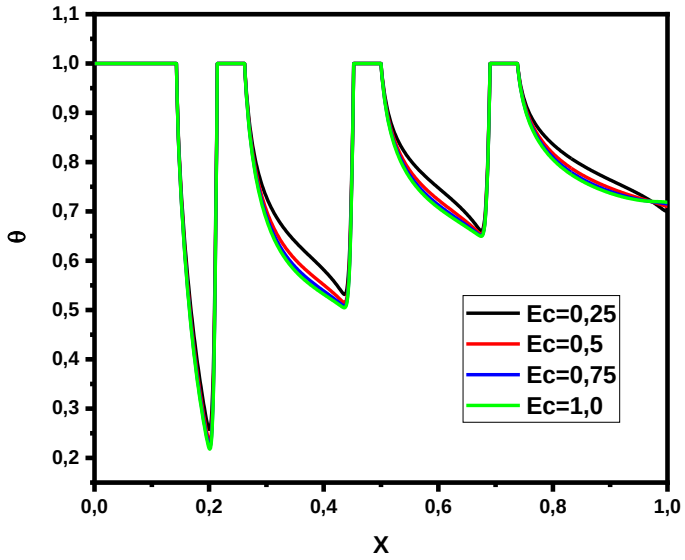

Fig. 22. Variation of θ (X;0.5) for different Eckert number at Re=50; Ha=25; ϕ=0.02

Figure 23 shows the influence of the Eckert number on the total entropy generation (Sgen) and the Bejan number (Be). The results indicated that the total entropy generation is augmented, and the Bejan number is reduced when the value of Eckert number (Ec) is increased. This effect is more noticeable at high values of Hartmann numbers. It is due to the enhancement of the entropy generation term associated with the magnetic field irreversibility and the term relative to the heat transfer irreversibility. It is indicated that the total entropy generation depends directly on the viscous dissipation and the external magnetic field.

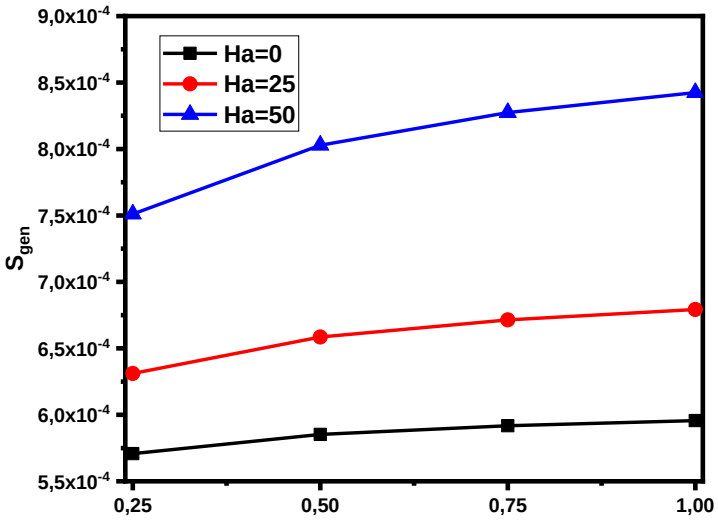

(a)

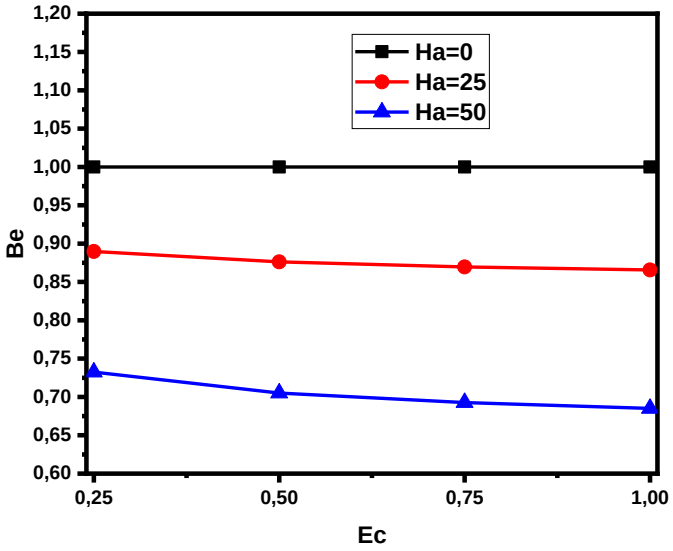

(b)

Fig. 23. Variation of the total entropy generation (a)and the Bejan number (b) for different Eckert number at Re=50; Ha=25; ϕ=0.02

4.7 Effects of Nanoparticles Volume Fraction

Figure 24 shows the effect of volume fractions of the nanoliquid on streamlines and isotherms for Re=50; Ha=0; Ec=0.5. From this figure, the streamlines of pure liquid are represented by a continuous line, and those for the nanoliquid are represented by a dashed line. It is noticeable that the streamlines of the nanoliquid are more compressed.

This figure demonstrates that the nanoliquid flow was approaching the cylindrical blocks, the streamlines were deflected toward the hot wall. The maximum value of the stream function is equal to (Ψmax=474.588) detected for pure water. The addition of nanoparticles in water decreases the value of stream function. This is due to the diminishing of the velocity flow of nanoliquid (cu-water).

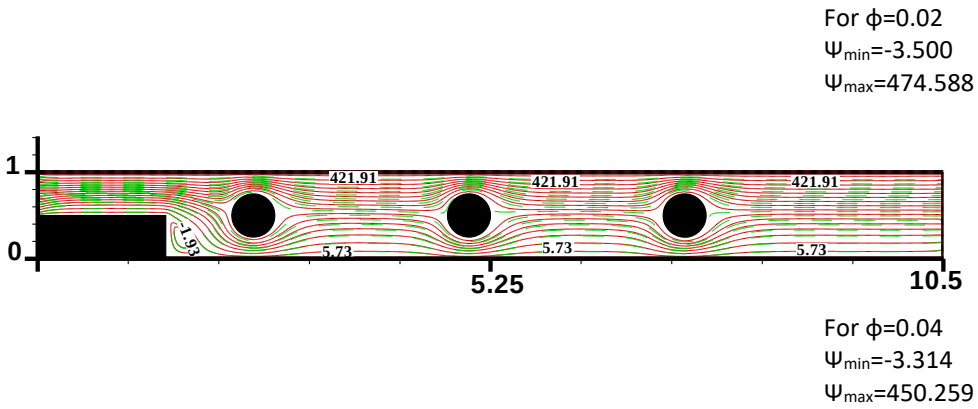

Fig. 24. Streamlines and isotherms contours for ϕ=0.04at Re=50; Ha=0; Ec=0.5

Figure 25 and Figure 26 shows the effect of volume fractions of the nanoliquid on the average and local Nusselt numbers for Re=50-100-150; Ha=0; Ec=0.5. The average and local Nusselt numbers increase with the increasing of nanoparticles volume concentration in nanoliquid. The average Nusselt number increases linearly, and the maximum value detected for ($\boldsymbol{\phi = 0.04}$), the addition of

nanoparticle in pure liquid enhances the heat transfer by about 7% for Re=50. The reason of this physical phenomenon can be attributed to two factors: the heightened thermal conductivity of the nanoliquid and the enlarged surface area of nanoparticles. This suggests that using nanoliquid is beneficial for improving heat transfer.

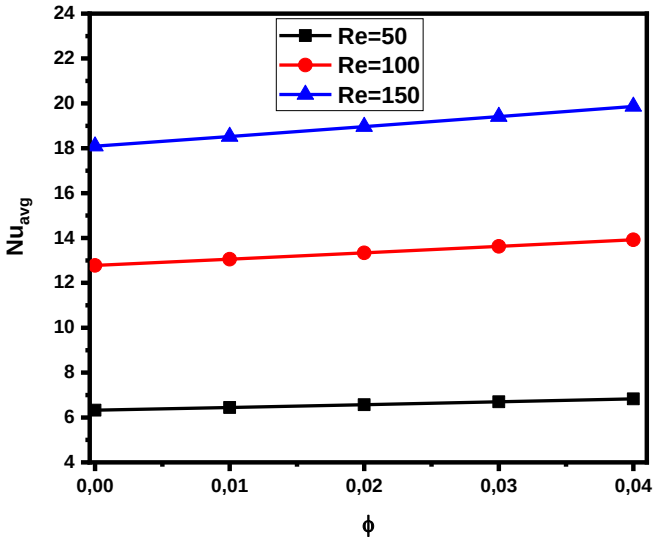

Fig. 25. Variation of Nu_{avg} in function of nanoparticle volume fraction for Re=50-100-150; Ha=0; Ec=0.5

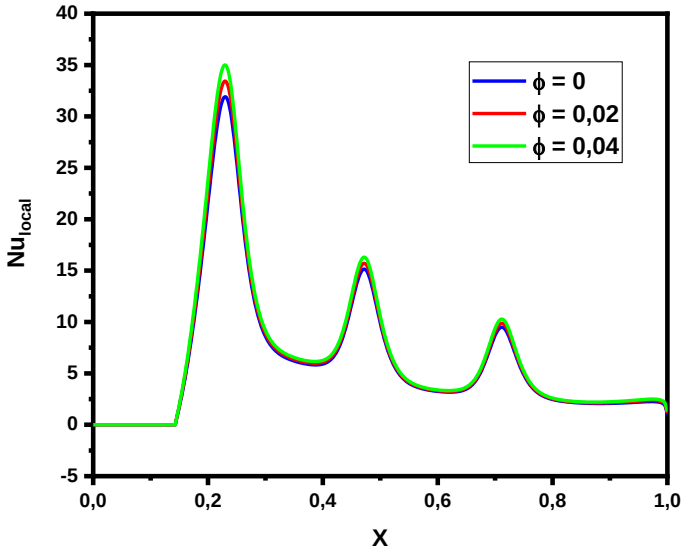

Fig. 26. Variation of Nu_{local} for different nanoparticle volume fraction at Re=50; Ha=0; Ec=0.5

The influence of nanoparticle volume fraction on the total entropy generation and the Bejan number for Re=50-100-150-200; Ha=0; Ec=0.5 is shown in Figure 27. Accordingly, as the nanoparticle volume fraction increases, the total entropy generation increases linearly and the Bejan number decreases. It is due to the additional sources of irreversibility introduced by nanoparticles. This means that there is a direct and proportional relationship between the total entropy generation and nanoparticle volume concentration. It can be explained by the improvement of the term relative to heat transfer irreversibility. It can be concluded that the addition of nanoparticles increases the thermal conductivity of the liquid, which enhances heat transfer between the nanoliquid and the

surrounding surfaces, leading to higher thermal irreversibility and entropy generation. Also, this is due to the presence of solid type nanoparticles in the base liquid.

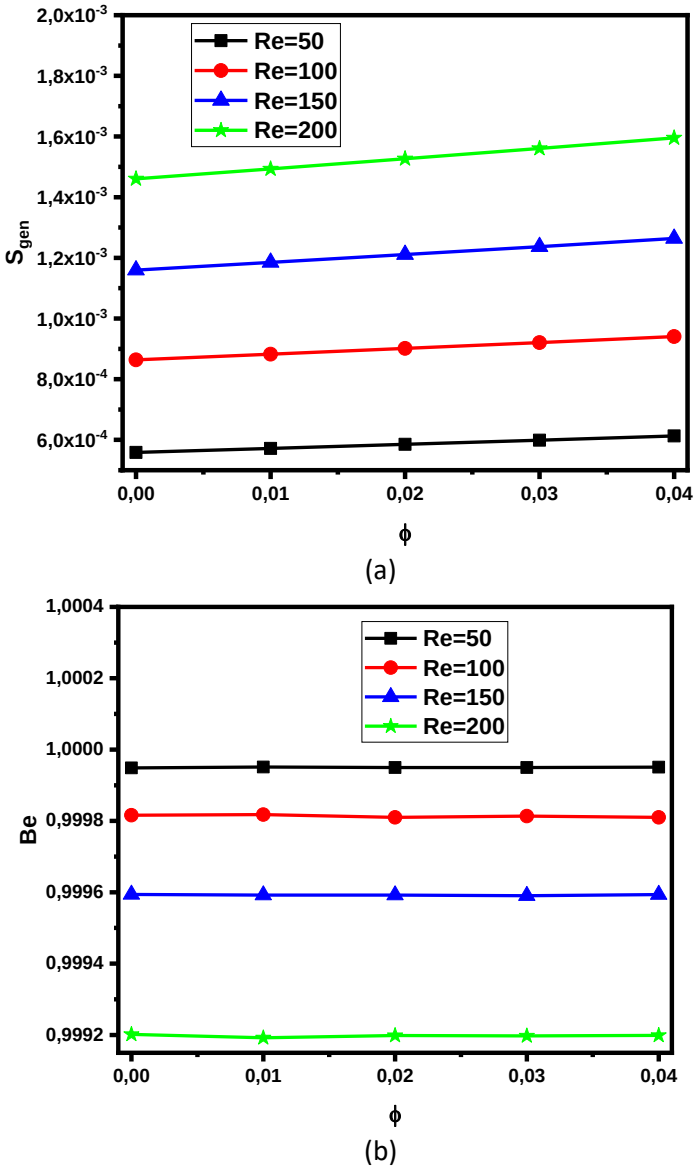

Fig. 27. Variation of the total entropy generation (a) and the Bejan number (b) for different nanoparticle volume fraction at Re=50-100-150-200; Ha=0; Ec=0

5. Conclusions

In this research, laminar MHD forced convection flow of a nanoliquid in a channel with an extended surface and three cylindrical blocks, in the presence of viscous dissipation. The imposed magnetic field was assumed to be uniform and constant. The LBM approach was used for simulation of nanoliquid laminar flow and heat transfer.

The interest was focused on the influence of the Reynolds number (Re), magnetic field (Ha), viscous dissipation (Ec) and nanoparticles volume fraction on streamlines and isotherms contours, local and average Nusselt number, velocity and the temperature profile, the total entropy generation (Sgen) and the Bejan number (Be). The main findings of this study can be summarized as follows:

i. The value of the stream function is enhanced significantly as the Reynolds number, Hartmann number, Eckert number are reduced with the addition of nanoparticles.
ii. Heat transfer of nanoliquid in terms of local and average Nusselt number is ameliorated when the value of Reynolds number, Eckert number, and nanoparticles volume fraction is enhanced. And it decreased when Hartmann's numbers increased. The heat transfer depends directly on the inertial force, Lorenz force, and viscous dissipation.
iii. The evolution of the heat transfer rate reaches up to 7% when 0.04 of the nanoparticles is added to the liquid. This confirms the effectiveness of using nanoparticles.
iv. The translation of the upper wall leads to an improvement in the heat transfer rate.
v. The velocity profile component increased with Reynolds number and Eckert number while it decreased with an increasing Hartmann number.
vi. The temperature profile component of nanoliquid decreases with Reynolds number, Hartmann number, Eckert number.
vii. The irreversibility represented by the total entropy generation increases according to the Reynolds number, Hartmann number, Eckert number and nanoparticles volume fraction.
viii. The irreversibility of nanoliquid depends on the inertial force, magnetic force, viscous dissipation term, conductivity and nanoparticles concentration.
ix. The bean number is reduced with high values of Reynolds number, Hartmann number, Eckert number and nanoparticles volume fraction.

As a future work, we can study the effect of multi-magnetic field on the heat transfer rate. Also, we can extrapolate this study to the case of nanoliquid flow in porous media.

Acknowledgement
This work was supported by the Tunisian Ministry of Higher Education and Scientific Research under grant 20/PRD-22.

References

[1] Choi, S. US, and Jeffrey A. Eastman. *Enhancing thermal conductivity of fluids with nanoparticles*. No. ANL/MSD/CP-84938; CONF-951135-29. Argonne National Lab.(ANL), Argonne, IL (United States), 1995. https://www.osti.gov/biblio/196525
[2] Esfe, Mohammad Hemmat, Wei-Mon Yan, Mohammad Akbari, Arash Karimipour, and Mohsen Hassani. "Experimental study on thermal conductivity of DWCNT-ZnO/water-EG nanofluids." *International Communications in Heat and Mass Transfer* 68 (2015): 248-251. https://doi.org/10.1016/j.icheatmasstransfer.2015.09.001
[3] Bazdidi-Tehrani, Farzad, Seyed Iman Vasefi, and Amir Masoud Anvari. "Analysis of particle dispersion and entropy generation in turbulent mixed convection of CuO-water nanofluid." *Heat Transfer Engineering* 40, no. 1-2 (2019): 81-94. https://doi.org/10.1080/01457632.2017.1404828
[4] Hemmat Esfe, Mohammad, Seyfolah Saedodin, Wei-Mon Yan, Masoud Afrand, and Nima Sina. "Study on thermal conductivity of water-based nanofluids with hybrid suspensions of CNTs/Al 2 O 3 nanoparticles." *Journal of Thermal Analysis and Calorimetry* 124 (2016): 455-460. https://link.springer.com/article/10.1007/s10973-015-5104-0
[5] Bahiraei, Mehdi, Saeed Heshmatian, and Mansour Keshavarzi. "Multi-attribute optimization of a novel micro liquid block working with green graphene nanofluid regarding preferences of decision maker." *Applied Thermal Engineering* 143 (2018): 11-21. https://doi.org/10.1016/j.applthermaleng.2018.07.074
[6] Bazdidi-Tehrani, Farzad, Arash Khabazipur, and Seyed Iman Vasefi. "Flow and heat transfer analysis of TiO2/water nanofluid in a ribbed flat-plate solar collector." *Renewable energy* 122 (2018): 406-418. https://doi.org/10.1016/j.renene.2018.01.056
[7] Vasefi, Seyed Iman, Farzad Bazdidi-Tehrani, Mohammad Sedaghatnejad, and Arash Khabazipur. "Optimization of turbulent convective heat transfer of CuO/water nanofluid in a square duct: An artificial neural network analysis." *Journal of Thermal Analysis and Calorimetry* 138 (2019): 517-529. https://link.springer.com/article/10.1007/s10973-019-08128-5

[8] Bahiraei, Mehdi, and Saeed Heshmatian. "Efficacy of a novel liquid block working with a nanofluid containing graphene nanoplatelets decorated with silver nanoparticles compared with conventional CPU coolers." *Applied Thermal Engineering* 127 (2017): 1233-1245.. https://doi.org/10.1016/j.applthermaleng.2017.08.136

[9] Abbassi, Mohamed Ammar, Mohammad Reza Safaei, Ridha Djebali, Kamel Guedri, Belkacem Zeghmati, and Abdullah AAA Alrashed. "LBM simulation of free convection in a nanofluid filled incinerator containing a hot block." *International Journal of Mechanical Sciences* 144 (2018): 172-185. https://doi.org/10.1016/j.ijmecsci.2018.05.031

[10] Abbassi, Mohamed Ammar, Ridha Djebali, and Kamel Guedri. "Effects of heater dimensions on nanofluid natural convection in a heated incinerator shaped cavity containing a heated block." *Journal of Thermal Engineering* 4, no. 3 (2018): 2018-2036. https://dx.doi.org/10.18186/journal-of-thermal-engineering.411434

[11] Miri, Rached, Mohamed A. Abbassi, Mokhtar Ferhi, and Ridha Djebali. "Second law analysis of mhd forced convective nanoliquid flow through a two-dimensional channel." *acta mechanica et automatica* 16, no. 4 (2022). https://sciendo.com/it/article/10.2478/ama-2022-0050

[12] Mliki, Bouchmel, Mohamed Ammar Abbassi, Ahmed Omri, and Zeghmati Belkacem. "Lattice Boltzmann analysis of MHD natural convection of CuO-water nanofluid in inclined C-shaped enclosures under the effect of nanoparticles Brownian motion." *Powder Technology* 308 (2017): 70-83. https://doi.org/10.1016/j.powtec.2016.11.054

[13] Halim, Nur Fazlin Che, and Nor Azwadi Che Sidik. "Nanorefrigerants: A Review on Thermophysical Properties and Their Heat Transfer Performance." *Journal of Advanced Research in Applied Sciences and Engineering Technology* 20, no. 1 (2020): 42-50. https://doi.org/10.37934/araset.20.1.4250

[14] Talib, Abd Rahim Abu, Sadeq Salman, Muhammad Fitri Mohd Zulkeple, and Ali Kareem Hilo. "Experimental Investigation of Nanofluid Turbulent Flow Over Microscale Backward-Facing Step." *Journal of Advanced Research in Fluid Mechanics and Thermal Sciences* 99, no. 2 (2022): 119-134. https://doi.org/10.37934/arfmts.99.2.119134

[15] Khairul, Mohammad A., Mohammad A. Alim, Islam M. Mahbubul, Rahman Saidur, Arif Hepbasli, and Altab Hossain. "Heat transfer performance and exergy analyses of a corrugated plate heat exchanger using metal oxide nanofluids." *International Communications in Heat and Mass Transfer* 50 (2014): 8-14. https://doi.org/10.1016/j.icheatmasstransfer.2013.11.006

[16] Barzegarian, Ramtin, Mostafa Keshavarz Moraveji, and Alireza Aloueyan. "Experimental investigation on heat transfer characteristics and pressure drop of BPHE (brazed plate heat exchanger) using TiO2–water nanofluid." *Experimental Thermal and Fluid Science* 74 (2016): 11-18. https://doi.org/10.1016/j.expthermflusci.2015.11.018

[17] Omiddezyani, S., I. Khazaee, S. Gharehkhani, M. Ashjaee, F. Shemirani, and V. Zandian. "Experimental Investigation of Convective Heat Transfer of Ferro-Nanofluid Containing Graphene in a Circular Tube under Magnetic Field." *Modares Mechanical Engineering* 19, no. 8 (2019): 1929-1941. https://mme.modares.ac.ir/article-15-27179-en.html

[18] Huang, Dan, Zan Wu, and Bengt Sunden. "Pressure drop and convective heat transfer of Al2O3/water and MWCNT/water nanofluids in a chevron plate heat exchanger." *International journal of heat and mass transfer* 89 (2015): 620-626. https://doi.org/10.1016/j.ijheatmasstransfer.2015.05.082

[19] Elfaghi, Abdulhafid MA, Alhadi A. Abosbaia, Munir FA Alkbir, and Abdoulhdi AB Omran. "CFD Simulation of Forced Convection Heat Transfer Enhancement in Pipe Using Al2O3/Water Nanofluid." *Journal of Advanced Research in Numerical Heat Transfer* 8, no. 1 (2022): 44-49.

[20] Razali, Nizamuddin, Mohd Bekri Rahim, and Sri Sumarwati. "Influence of Volume Fraction of Titanium Dioxide Nanoparticles on the Thermal Performance of Wire and Tube of Domestic Refrigerator Condenser Operated with Nanofluid." *Journal of Advanced Research in Numerical Heat Transfer* 11, no. 1 (2022): 12-22.

[21] Karimipour, Arash, Abdolmajid Taghipour, and Amir Malvandi. "Developing the laminar MHD forced convection flow of water/FMWNT carbon nanotubes in a microchannel imposed the uniform heat flux." *Journal of Magnetism and Magnetic Materials* 419 (2016): 420-428. https://doi.org/10.1016/j.jmmm.2016.06.063

[22] Sheikholeslami, M., and M. M. Bhatti. "Forced convection of nanofluid in presence of constant magnetic field considering shape effects of nanoparticles." *International Journal of Heat and Mass Transfer* 111 (2017): 1039-1049. https://doi.org/10.1016/j.ijheatmasstransfer.2017.04.070

[23] Aminossadati, S. M., A. Raisi, and B. Ghasemi. "Effects of magnetic field on nanofluid forced convection in a partially heated microchannel." *International Journal of Non-Linear Mechanics* 46, no. 10 (2011): 1373-1382. https://doi.org/10.1016/j.ijnonlinmec.2011.07.013

[24] Hamad, M. A. A., I. Pop, and Al Md Ismail. "Magnetic field effects on free convection flow of a nanofluid past a vertical semi-infinite flat plate." *Nonlinear Analysis: Real World Applications* 12, no. 3 (2011): 1338-1346. https://doi.org/10.1016/j.nonrwa.2010.09.014

[25] Sheikholeslami, Mohsen, Kuppalapalle Vajravelu, and Mohammad Mehdi Rashidi. "Forced convection heat transfer in a semi annulus under the influence of a variable magnetic field." *International journal of heat and mass transfer* 92 (2016): 339-348. https://doi.org/10.1016/j.ijheatmasstransfer.2015.08.066

[26] Selimefendigil, Fatih, Hakan F. Öztop, and Ali J. Chamkha. "Role of magnetic field on forced convection of nanofluid in a branching channel." *International Journal of Numerical Methods for Heat & Fluid Flow* 30, no. 4 (2020): 1755-1772. https://doi.org/10.1108/HFF-10-2018-0568

[27] Ishak, Anuar, Roslinda Nazar, and Ioan Pop. "MHD convective flow adjacent to a vertical surface with prescribed wall heat flux." *International Communications in Heat and Mass Transfer* 36, no. 6 (2009): 554-557. https://doi.org/10.1016/j.icheatmasstransfer.2009.02.012

[28] Selimefendigil, Fatih, and Hakan F. Öztop. "Magnetic field effects on the forced convection of CuO-water nanofluid flow in a channel with circular cylinders and thermal predictions using ANFIS." *International Journal of Mechanical Sciences* 146 (2018): 9-24. https://doi.org/10.1016/j.ijmecsci.2018.07.011

[29] Manvi, Bharatkumar, Jagadish Tawade, Mahadev Biradar, Samad Noeiaghdam, Unai Fernandez-Gamiz, and Vediyappan Govindan. "The effects of MHD radiating and non-uniform heat source/sink with heating on the momentum and heat transfer of Eyring-Powell fluid over a stretching." *Results in Engineering* 14 (2022): 100435. https://doi.org/10.1016/j.rineng.2022.100435

[30] Sharma, Madhu, Bhupendra K. Sharma, Umesh Khanduri, Nidhish K. Mishra, Samad Noeiaghdam, and Unai Fernandez-Gamiz. "Optimization of heat transfer nanofluid blood flow through a stenosed artery in the presence of Hall effect and hematocrit dependent viscosity." *Case Studies in Thermal Engineering* 47 (2023): 103075. https://doi.org/10.1016/j.csite.2023.103075

[31] Das, S., S. Chakraborty, and R. N. Jana. "Entropy analysis of Poiseuille nanofluid flow in a porous channel with slip and convective boundary conditions under magnetic field." *World Journal of Engineering* 18, no. 6 (2021): 870-885. https://doi.org/10.1108/WJE-12-2020-0660

[32] Das, S., A. S. Banu, R. N. Jana, and O. D. Makinde. "Hall current's impact on ionized ethylene glycol containing metal nanoparticles flowing through vertical permeable channel." *Journal of Nanofluids* 11, no. 3 (2022): 453-467. https://doi.org/10.1166/jon.2022.1842

[33] Das, S., S. Sarkar, and R. N. Jana. "Entropy generation minimization of magnetohydrodynamic slip flow of casson H2O+ Cu nanofluid in a porous microchannel." *Journal of Nanofluids* 8, no. 1 (2019): 205-221. https://doi.org/10.1166/jon.2019.1554

[34] Mahmood, Zafar, Umar Khan, S. Saleem, Khadija Rafique, and Sayed M. Eldin. "Numerical analysis of ternary hybrid nanofluid flow over a stagnation region of stretching/shrinking curved surface with suction and lorentz force." *Journal of Magnetism and Magnetic Materials* 573 (2023): 170654. https://doi.org/10.1016/j.jmmm.2023.170654

[35] Khan, Umar, Zafar Mahmood, Sayed M. Eldin, Basim M. Makhdoum, Bandar M. Fadhl, and Ahmed Alshehri. "Mathematical analysis of heat and mass transfer on unsteady stagnation point flow of Riga plate with binary chemical reaction and thermal radiation effects." *Heliyon* 9, no. 3 (2023). https://doi.org/10.1016/j.heliyon.2023.e14472

[36] Makhdoum, Basim M., Zafar Mahmood, Umar Khan, Bandar M. Fadhl, Ilyas Khan, and Sayed M. Eldin. "Impact of suction with nanoparticles aggregation and joule heating on unsteady MHD stagnation point flow of nanofluids over horizontal cylinder." *Heliyon* 9, no. 4 (2023).https://doi.org/10.1016/j.heliyon.2023.e15012

[37] Aydın, Orhan, and Mete Avcı. "Laminar forced convection with viscous dissipation in a Couette–Poiseuille flow between parallel plates." *Applied energy* 83, no. 8 (2006): 856-867. https://doi.org/10.1016/j.apenergy.2005.08.005

[38] Das, S., S. Sarkar, and R. N. Jana. "Feature of entropy generation in Cu-Al 2 O 3/ethylene glycol hybrid nanofluid flow through a rotating channel." *Bionanoscience* 10 (2020): 950-967. https://doi.org/10.1007/s12668-020-00773-7

[39] Jaber, Khaled K. "Effects of viscous dissipation and Joule heating on MHD flow of a fluid with variable properties past astretching vertical plate." *European Scientific Journal* 10, no. 33 (2014). https://doi.org/10.19044/esj.2014.v10n33p%25p.

[40] Mousavi, S. Morteza, Bahman Ehteshami, and A. Ali Rabienataj Darzi. "Two-and-three-dimensional analysis of Joule and viscous heating effects on MHD nanofluid forced convection in microchannels." *Thermal Science and Engineering Progress* 25 (2021): 100983. https://doi.org/10.1016/j.tsep.2021.100983

[41] Sheikholeslami, Mohsen, Shirley Abelman, and Davood Domiri Ganji. "Numerical simulation of MHD nanofluid flow and heat transfer considering viscous dissipation." *International Journal of Heat and Mass Transfer* 79 (2014): 212-222. https://doi.org/10.1016/j.ijheatmasstransfer.2014.08.004

[42] Mehmood, Ahmer, and Asif Ali. "Analytic solution of three-dimensional viscous flow and heat transfer over a stretching flat surface by homotopy analysis method." (2008): 121701. https://doi.org/10.1115/1.2969753

[43] Arulmozhi, S., K. Sukkiramathi, Shyam Sundar Santra, R. Edwan, Unai Fernandez-Gamiz, and Samad Noeiaghdam. "Heat and mass transfer analysis of radiative and chemical reactive effects on MHD nanofluid over an infinite moving vertical plate." *Results in Engineering* 14 (2022): 100394. https://doi.org/10.1016/j.rineng.2022.100394

[44] Guled, C. N., J. V. Tawade, P. Kumam, S. Noeiaghdam, I. Maharudrappa, S. M. Chithra, and V. Govindan. "The heat transfer effects of MHD slip flow with suction and injection and radiation over a shrinking sheet by optimal homotopy analysis method." *Results in Engineering* 18 (2023): 101173. https://doi.org/10.1016/j.rineng.2023.101173

[45] Atashafrooz, M., H. Sajjadi, A. Amiri Delouei, Tien-Fu Yang, and Wei-Mon Yan. "Three-dimensional analysis of entropy generation for forced convection over an inclined step with presence of solid nanoparticles and magnetic force." *Numerical Heat Transfer, Part A: Applications* 80, no. 6 (2021): 318-335. https://doi.org/10.1080/10407782.2021.1944579

[46] Rafique, Khadija, Zafar Mahmood, S. Saleem, Sayed M. Eldin, and Umar Khan. "Impact of nanoparticle shape on entropy production of nanofluid over permeable MHD stretching sheet at quadratic velocity and viscous dissipation." *Case Studies in Thermal Engineering* 45 (2023): 102992. https://doi.org/10.1016/j.csite.2023.102992

[47] Rafique, Khadija, Zafar Mahmood, Haifa Alqahtani, and Sayed M. Eldin. "Various nanoparticle shapes and quadratic velocity impacts on entropy generation and MHD flow over a stretching sheet with joule heating." *Alexandria Engineering Journal* 71 (2023): 147-159. https://doi.org/10.1016/j.aej.2023.03.021

[48] Makhdoum, Basim M., Zafar Mahmood, Bandar M. Fadhl, Musaad S. Aldhabani, Umar Khan, and Sayed M. Eldin. "Significance of entropy generation and nanoparticle aggregation on stagnation point flow of nanofluid over stretching sheet with inclined Lorentz force." *Arabian Journal of Chemistry* 16, no. 6 (2023): 104787. https://doi.org/10.1016/j.arabjc.2023.104787

[49] Atashafrooz, M., M. Sheikholeslami, H. Sajjadi, and A. Amiri Delouei. "Interaction effects of an inclined magnetic field and nanofluid on forced convection heat transfer and flow irreversibility in a duct with an abrupt contraction." *Journal of Magnetism and Magnetic Materials* 478 (2019): 216-226. https://doi.org/10.1016/j.jmmm.2019.01.111

[50] Santra, Apurba Kumar, Swarnendu Sen, and Niladri Chakraborty. "Study of heat transfer due to laminar flow of copper–water nanofluid through two isothermally heated parallel plates." *International journal of thermal sciences* 48, no. 2 (2009): 391-400. https://doi.org/10.1016/j.ijthermalsci.2008.10.004

[51] Ferhi, Mokhtar, and R. I. D. H. A. Djebali. "Heat transfer appraising and second law analysis of Cu-water nanoliquid filled microchannel: Slip flow regime." *Romanian Journal of Physics* 67 (2022): 605. https://rjp.nipne.ro/2022_67_1-2.html